2016

Investigating DNA Binding of Histone-Derived Antimicrobial Peptides, Buforin II and DesHDAP1, for Effective Peptide Design

Sukin Sim
ssim2@wellesley.edu

Investigating DNA Binding of Histone-Derived Antimicrobial Peptides, Buforin II and DesHDAP1, for Effective Peptide Design

Sukin Sim

Submitted in Partial Fulfillment
of the
Prerequisite for Honors
in Chemical Physics

Advisor: Donald Elmore

April 2016

Abstract

Antimicrobial peptides (AMPs), which are found in numerous living organisms, are active against a wide range of bacteria and other pathogens, making them promising candidates for alternatives to conventional antibiotics. While many AMPs inhibit bacterial growth through membrane disruption, some AMPs, including buforin II and DesHDAP1, are hypothesized to kill bacteria by binding intracellular nucleic acids after translocating across the bacterial cell membrane without significant membrane permeabilization. To understand this lesser known mechanism, the peptide-DNA binding interactions of these peptides were investigated using several computational and experimental methods. Results from analyzing molecular dynamics (MD) simulations of buforin II-DNA and DesHDAP1-DNA complexes suggested that the DNA binding of buforin II and DesHDAP1 was not base selective as these peptides interacted primarily with the phosphate groups of the DNA backbone. Following these simulations, an alternative computational method, electrostatic calculations via component analysis, as well as a fluorescence intercalator displacement (FID) assay were used to confirm our prediction on the lack of base selectivity. This combination of computational and experimental methods was used again to explore the effects of arginine residues in DNA binding as previous work has suggested arginine's important role in protein-membrane interactions and antimicrobial activities of buforin II and DesHDAP1. In both experiments and calculations, having an increased composition of cationic residues that are arginine instead of lysine were shown to promote binding for variants of both buforin II and DesHDAP1. These insights regarding DNA binding of buforin II and DesHDAP1, paired with a deeper understanding of the peptides' structures and membrane interactions, are necessary for development of more potent analogs which may lead to novel pharmaceutical applications.

Acknowledgements

First, I would like to thank my research advisor, Don, for his guidance and support since my first year at Wellesley. By working as a member of his lab for almost four years, I developed a deeper appreciation and interest in science and research. Don has encouraged me to become more independent and helped me grow as a student and scientist.

I would also like to thank Mala, who has encouraged me to pursue chemistry since my first year. I am grateful for all her help, such as when she taught me new computational techniques to improve my research.

In addition, I would like to thank my thesis committee, Professors James Battat and Ellen Hildreth, for helping me with the thesis process.

I would also like to thank my fellow Elmore lab members for helping me learn new techniques, letting me use their peptide solutions, and providing encouragement and support.

Last but not least, I would like to thank and acknowledge my family and friends for their emotional support. I would especially like to thank the Glass Room Crew for regularly staying up with me at the science center until 2 a.m., Jane Zhu ’16 for being my partner for countless problem sets and final projects but mostly for being an amazing friend, and Frieda Zhang ’15 for being a close friend and role model.

Contents

1. Introduction

1.1 Antimicrobial Peptides (AMPs)

While antibiotic and antimicrobial agents have treated numerous infectious diseases over the years, the rapidly growing resistance to these drugs is becoming a global concern [1-4]. This prompts a need for alternatives to conventional antibiotics to provide effective treatments of resistant infections and diseases. Fortunately, antimicrobial peptides (AMPs) may be a potential class of alternatives to conventional antibiotics as many species of AMPs have been studied and shown to be active against a wide range of bacteria, viruses, and other pathogens [5].

AMPs are generally cationic, amphipathic, and fewer than 100 amino acid residues in length. In addition, they are naturally occurring in many organisms, including humans, as part of the innate immune system [4]. Thus, a better understanding of these peptides, particularly their structure-function relationships, may be crucial for development of novel agents or treatments against drug-resistant pathogens.

Peptide	Proposed Mechanism of Action
Lasioglosin II (LL-II) [4]	Membrane destabilization
pseudin-2 [6]	Formation of pores
Gaegurin 4 [4]	Formation of pores
Cecropin A [4]	Formation of pores
AMP-C10-3 [3]	Membrane permeabilization
Indolicidin [7]	Formation of pores
Magainin-2 [7]	Formation of pores
Tachyplesin I [7]	Formation of pores

Table 1. Examples of AMPs that kill bacteria by destabilizing the membrane integrity.

According to the literature, many AMPs have been shown to kill bacteria through membrane disruption or permeabilization, with some examples shown in Table 1. Several

models, including the barrel-stave, toroidal, and carpet models, were proposed to describe this permeabilization mechanism [8]. The barrel-stave model involves AMPs binding the membrane surface as monomers, followed by aggregation of these peptides that eventually forms transmembrane pores. As the concentration of AMPs increases, these pores become larger, ultimately causing cell death through leakage [9]. Examples of AMPs that follow this mechanism include Gaegurin 4 and Cecropin A [4]. Unlike the former model, according to the toroidal model, AMPs insert themselves in the membrane until it becomes interdispersed with peptides. This then causes strain and thinning of the membrane, effectively destabilizing the membrane integrity. This model well characterizes peptide-membrane interactions as mechanisms of several AMPs, such as meganin, protegrin, and melittin, have been shown to follow this model [9]. Lastly, unlike the other two models, AMPs following the carpet model do not form any pores or channels but instead engage in nonspecific interactions with the membrane as they accumulate near the surface due to electrostatic interactions. This accumulation then leads to the loss of membrane integrity. Though these mechanisms are different on the small scale, they all ultimately kill bacteria by impairing the integrity of the bacterial membrane.

While many AMPs kill via permeabilization, a smaller subset of AMPs causes cell damage or death by translocating across the membrane with minimal permeabilization; once inside the cell, these AMPs then interfere with intracellular processes (Figure 1).

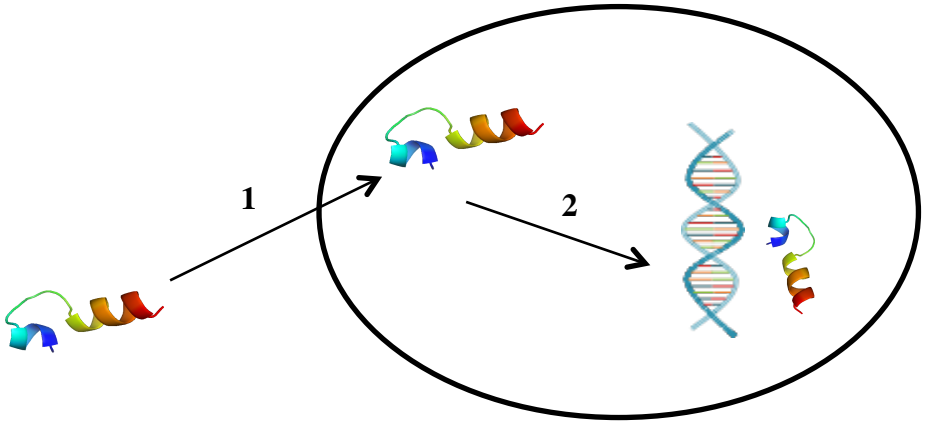

Figure 1. This lesser known bactericidal mechanism involves (1) translocation across bacterial membrane followed by (2) interference with crucial intracellular processes.

These intracellular processes may refer to interactions with specific proteins or nucleic acids. Buforin II and DesHDAP1, the two subjects of this study, follow this lesser understood mechanism. However, their mechanism of action is not considered unique as several other peptides were shown to share at least parts of the proposed mechanism. For example, peptides such as polyphemusin I and a 9-amino-acid-long motif with sequence PLIYLRLLR were discovered to be translocating peptides, with the latter found to spontaneously translocate across membranes carrying polar dyes [7, 10]. An even greater number of peptides that bind nucleic acids were identified in Table 2.

Peptide	
Lasioglosin II (LL-II)	DNA binding
pseudin-2	RNA binding
AMP-C10-3	DNA binding
LL-37	DNA binding
PuroB peptides	DNA and RNA binding

Table 2. Examples of peptides that have been proposed to bind nucleic acids.

It is important to note that while some of these peptides listed in Table 2 may bind nucleic acids as part of their mechanism to kill pathogens, some may also have been seen *in vitro* to bind

DNA, which is expected for cationic peptides. Nonetheless, it is important to understand alternative mechanisms, which could be useful for development of agents that can deliver drug molecules or other desired cargos such as nucleic acids, to target cells [11, 12]. In addition, Table 1 and Table 2 share common peptides, which means mechanisms of AMPs are not only limited to the two mentioned earlier. That is, mechanisms of AMPs may be more complex and "multifunctional" [3]. Therefore, our study aims to provide a more thorough characterization of the nucleic acid binding step through analysis of buforin II and DesHDAP1.

1.2 Histone-Derived Antimicrobial Peptides (HDAPs)

Histones are found in eukaryotic cell nuclei, where they package DNA into more organized units called nucleosomes. Thus, these proteins are central to processes such as gene transcription and regulation in cells. In addition, some of the core histone proteins, as well as their fragments, were shown to be active against a wide range of antimicrobial agents. In the literature, histones and their fragments extracted from various organisms such as shrimp, fish, frog, chicken, and mammals showed potential for use as antimicrobial agents [8].

Histone-derived antimicrobial peptides (HDAPs) are generally short peptides (<100 amino acids in length), derived from histones and/or their fragments. In the literature, examples of HDAPS include a potential AMP derived from the histone H2A of the Zhikong scallop *Chlamys farreri* [8] and an active peptide found in coho salmon mucus and blood that shares its entire sequence with the N-terminus of trout H1 histone [13]. Buforin II and DesHDAP1, two more examples of HDAPs share their entire sequences with sections of histone H2A.

1.3 Buforin II

Buforin II is a well-characterized HDAP active against a wide range of pathogens including several Gram-positive and Gram-negative bacteria and fungi without significant hemolytic activity [14]. It is a 21-amino acid peptide that is cationic, amphipathic, and α-helical, its structure containing an N-terminal random coil region, extended helical region, a hinge, and a C-terminal α-helical region as shown in Figure 2 [8, 15, 16].

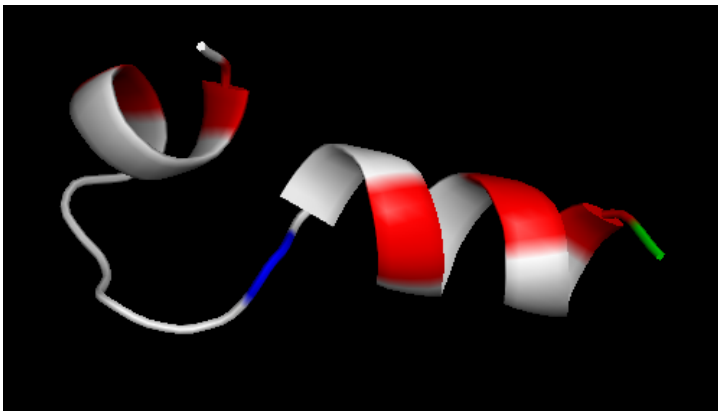

Figure 2. Structure of buforin II. Arginine residues shown in red, lysine residue shown in green, and proline residue shown in blue.

Buforin II is naturally occurring, derived from its parent AMP, buforin I, which was isolated from the stomach tissue of the Asian toad *Bufo bufo garagriozans* [14]. As a HDAP, buforin II shares its complete sequence with the N-terminal region of histone H2A that has been shown to interact with nucleic acids [16]. Past studies showed that though buforin II belongs to a class of linear α-helical AMPs, it has a unique mechanism of action that involves membrane translocation and interaction with intracellular DNA and RNA [14, 17].

Peptide	Sequence
Buforin II	TRSSRAGLQWPVGRVHRLLRK
DesHDAP1	ARDNKKTRIWPRHLQLAVRN

Table 3. Amino acid sequences of buforin II and DesHDAP1, the subjects of this study.

To better understand this lesser known mechanism, buforin II's membrane translocation and interaction with nucleic acids have been investigated in the past. Regarding the translocation step of buforin II's bactericidal mechanism, the proline hinge in the peptide structure was shown to be crucial to membrane translocation, which also affected its potency [14, 15, 18]. This proved translocation was a major step in buforin II's overall mechanism of action [15, 19]. Uyterhoeven et al. then used molecular modeling as well as a fluorescent intercalator displacement assay to better characterize the DNA binding of buforin II. According to this study, buforin II was observed to form nonspecific electrostatic interactions with the phosphate backbone of DNA while forming interactions with specific arginine residues. In addition, a general correlation between relative DNA binding constants and antimicrobial activity for buforin II and its variants was noted, supporting the hypothesis that buforin II kills bacteria via DNA binding [17]. Though this previous study has provided interesting observations and predictions, the MD simulation used to characterize the DNA binding of buforin II was only 10 ns long. While the length of simulation will be discussed later, 50 ns appeared to be an optimal amount of simulation time as systems in this study equilibrated at around 40 ns. In addition, Lan et al. discussed that the level of helical structure in the simulation was not consistent with their experimental results using circular dichroism spectroscopy. The single simulation used by Uyterhoeven et al. proposed that buforin II maintained an α-helical structure, whereas the result from CD spectroscopy suggested a more extended conformation [20]. Therefore, more replicates of extended MD simulations were run and analyzed in this study to explore a greater sampling of possible structures. Furthermore, not much is known regarding the DNA binding of DesHDAP1, the other peptide investigated in this study, though past studies have proposed that DesHDAP1's mechanism is similar to that of buforin II [21]. Therefore, a close study of nucleic acid binding of both

peptides is necessary using computational analyses as well as experimental methods to address past conclusions and predictions and gain further insight.

1.4 DesHDAP1

While buforin II is a naturally occurring peptide, DesHDAP1 is a 20-amino acid HDAP that was designed based on the crystal structure of the histone H2A subunit. Similar to buforin II, DesHDAP1 also shares its sequence identity with a section of the histone subunit H2A [1]. DesHDAP1 was designed based on properties of buforin II, and therefore, DesHDAP1 contains multiple positive charges and a proline residue in its structure that disrupts a C-terminal helical region [21].

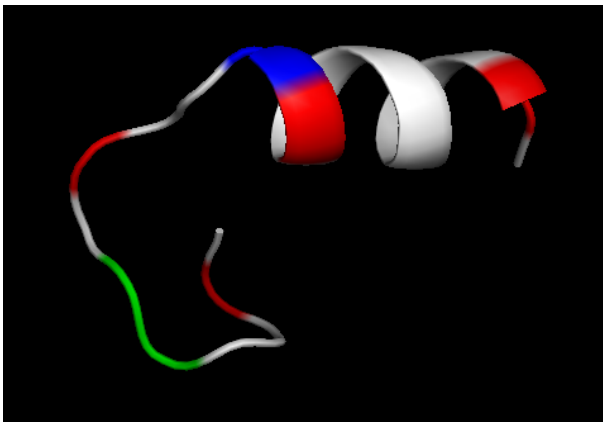

Figure 3. Structure of DesHDAP1. All arginine residues shown in red, lysine residues shown in green, and proline residue shown in blue.

Furthermore, a structural analysis using circular dichroism spectroscopy confirmed that DesHDAP1 and buforin II share similar secondary structures [1]. DesHDAP1 also exhibited comparable antimicrobial activity, and as mentioned earlier, past DNA binding and translocation studies suggested that DesHDAP1 likely shares buforin II's bactericidal mechanism [1, 21].

Because both buforin II's and DesHDAP1's modes of action involve nucleic acid binding following translocation across bacterial membrane, characterizing nucleic acid binding of these peptides may help us better understand this lesser known mechanism as well as provide insight such that we can optimize these translocating and binding abilities to engineer more potent peptides that can deliver drugs or cargos into target cells.

1.5 Classical Molecular Dynamics (CMD)

Classical molecular dynamics (CMD) is a computational tool used to investigate structure and function of complex biomolecules. CMD does not consider motions of electrons and instead uses classical physics to update positions of nuclei over time. Because MD simulations allow for close analysis of relatively large systems at the molecular level, it is used for a wide range of studies and applications, such as structural determinations of biomolecules.

Each atom in a MD simulation is assigned an initial value of position and velocity. Velocity on each atom is randomly selected from the Maxwell-Boltzmann distribution. The force on the atom is evaluated using a force field or classical potential energy function, an empirical formula of force on the atom that is effectively divided into bonded and non-bonded terms. The bonded terms consider effects of intramolecular interactions, including terms accounting for bonds, angles, and dihedrals, whereas the non-bonded terms consider effects of intermolecular interactions such as van der Waals and electrostatic interactions. These bonded and non-bonded terms use empirically and/or quantum mechanically derived parameters based on a certain set of molecules that may be the basis for many molecules, such as methyl groups. It is important to note that different force fields, created by collaborative efforts of various research groups, contain different terms. No force field is considered "true" or universal that applies to all

molecules. However, a particular force field can provide a model that is accurate for certain sets of molecules.

$$
\begin{aligned}
U = & \sum_{bonds} k_r (r - r_0)^2 \\
& + \sum_{angles} k_\theta (\theta - \theta_0)^2 \\
& + \sum_{dihedrals} k_\phi [1 + cos(n\phi + \phi_0)] \\
& + \sum_{atom\, i} \sum_{j \neq i} 4\epsilon_{i,j} \left[\left(\frac{\sigma_{i,j}}{r_{i,j}} \right)^{12} - \left(\frac{\sigma_{i,j}}{r_{i,j}} \right)^{6} \right] \\
& + \sum_{i} \sum_{j \neq i} \frac{q_i q_j}{\epsilon_0 r_{i,j}}
\end{aligned}
$$

Equation 1. Generic potential energy equation for the AMBER force field.
Using this function, we can compute the force on each atom using classical mechanics.

Thus, some force fields are better suited for simulating particular biomolecules, such as proteins and nucleic acids. For example, AMBER force fields have been shown to be particularly useful for modeling nucleic acids as they include updated parameters for both amino and nucleic acids [1, 17, 22-25]. After calculating the force using a force field, the atom moves over a small time step, on the order of femtoseconds (10^{-15} s), following Newton's laws in classical mechanics to its next position. The process of calculating updated positions and forces repeat over and over again up to a desired time length, creating a compilation or simulation of atomic movements to model the macroscopic behavior or dynamics of the molecule(s) in the system.

In some MD simulations, to model the effect of solvent, an explicit solvation model is used in which every solvent atom is considered in calculations. Though the explicit treatment of solvent makes these MD simulations computationally expensive, there are several instances in

which explicit solvation produces accurate results [26, 27]. In the literature, modeling comparable systems, for example a peptide nucleic acid targeting mRNA molecules, in explicit solvent produced results that agreed well with experimental data. For systems containing dynamic biomolecules such as proteins, MD appears to be a good technique to explore possible conformations to investigate different functions and behaviors. After a MD simulation is run, this produces numbers of "snapshots" or frames of the system of interest. With these snapshots, various computational analyses can be performed to check for structural stability, energetics, H-bonds, and other properties of the system.

1.6 Electrostatics

In biological systems, electrostatic interactions can heavily influence structure and dynamics of biomolecules by affecting affinity, specificity, and promiscuity [28]. For many biological systems, probing electrostatics can provide insight on function and interactions of biomolecules, which can be useful for applications such as drug design. Electrostatic interactions are sensitive to environmental factors such as salt concentration, pH, and presence of solvent, which are all very relevant in biological settings. To describe such interactions, an implicit solvent model can be used, in which the solvent is considered to be a medium with an associated dielectric constant. This is different from an explicit solvent model, which considers every atom in the solvent to model the effects. Thus, implicit consideration of the solvent involves solving the Poisson equation to obtain the electrostatic potential at a point in space, given the charge distribution $\rho(\vec{r})$ and the dielectric constant $\varepsilon(\vec{r})$ that vary in space.

$$-\nabla \cdot (\varepsilon(\vec{r})\nabla\phi(\vec{r})) = \frac{\rho(\vec{r})}{\varepsilon_0}$$

Equation 2. Poisson Equation.

To implicitly model effects of monovalent, mobile ions in solvent, the Poisson equation becomes the Poisson-Boltzmann equation (PBE) after applying Debye-Huckel theory [24]. Given that the system of interest is not heavily charged, we can approximate PBE to its linearized version (Equation 3) [24].

$$-\nabla \cdot (\varepsilon(\vec{r})\nabla\phi(\vec{r})) = \frac{\rho(\vec{r})}{\varepsilon_0} - \varepsilon(\vec{r})\kappa^2\phi(\vec{r})$$

Equation 3. Linearized approximation to the PBE.

Using the linearized PBE, or LPBE, a free energy can be calculated that represents the electrostatic component of the free energy of the system. Total electrostatic binding free energies are obtained by summing terms that account for penalties for solvating each binding partner (in other words, desolvating the spatial cavities of the binding partners) and solvent-screened interactions between the two partners (scheme shown in Figure 4).

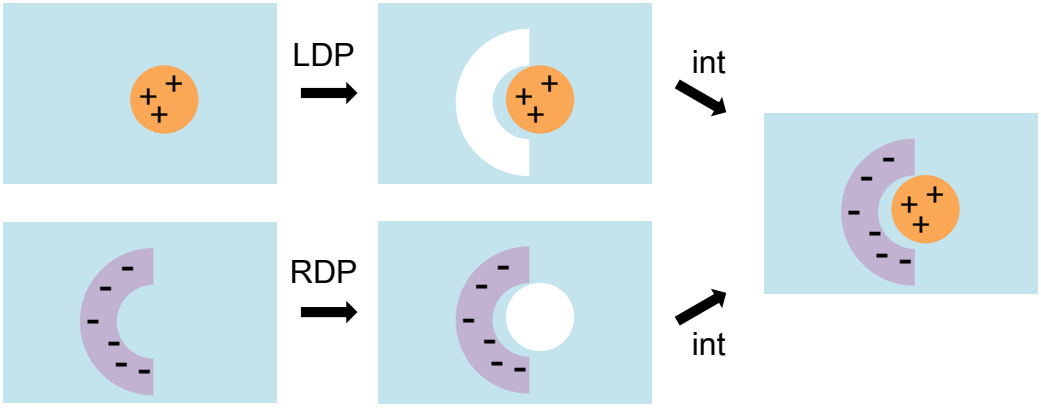

Figure 4. Scheme for calculating electrostatic component of binding free energy [28].

The penalty terms were obtained by multiplying one-half the potential differences due to charges on a binding partner by those charges. Interaction terms were calculated multiplying bound-state potentials due to charges on a binding partner by charges on the other partner [29].

$$\Delta G_{elec} = DP1 + DP2 + int$$

Equation 4. Total electrostatic binding free energy is a sum of desolvation penalties of partner #1 and #2 and the interactions term.

1.7 Component Analysis

To quantify the contributions of selected portions of a binding partner on the overall electrostatic binding free energy, atomic charges of these portions were set to zero followed by a recalculation of the binding free energy. The contribution of that portion, or the effect of zeroing out the charges of the portion, was reflected by the changes in the electrostatic binding free energy, ΔΔG, obtained by subtracting the binding energy with zeroed atomic charges from the original binding energy with all initial charges (Equation 5). Therefore, a positive ΔΔG implies that the portion or residue that has been zeroed is unfavorable to the overall binding, while a negative ΔΔG implies that the residue that was zeroed is favorable to binding.

$$\Delta\Delta G_{bind} = \Delta G_{bind,orig} - \Delta G_{bind,zeroed}$$

Equation 5. Equation to calculate contribution of a portion of a binding partner on the overall electrostatic component of the binding free energy. $\Delta G_{bind,orig}$ is the original binding energy, and $\Delta G_{bind,zeroed}$ is the binding energy after charges of a selected portion of a binding partner have been zeroed.

2. Methods and Materials

2.1 Molecular Modeling

To computationally characterize DNA interactions of HDAPs, initial models of buforin II and DesHDAP1 were extracted from the histone core particle crystal structure (1AOI) as shown in Figure 5, which was used in previous computational studies of buforin II [17, 30].

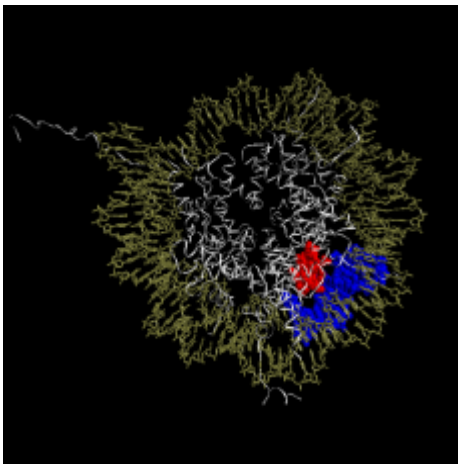

Figure 5. Crystal structure of histone H2A, where sequence of buforin II is shown in red. Adjacent dsDNA used in simulations is shown in blue. (Image created by Donald Elmore)

Each of these peptide-DNA complexes includes a particular section of the histone protein that shares an identical sequence as the peptide and an adjacent section of DNA in the original histone structure. For the complex containing buforin II, the adjacent section of DNA has 21 base pairs, and for the complex containing DesHDAP1, the adjacent section of DNA has 20 base pairs. All structures from modeling and experiments included a F10W mutation, which has been used in many previous studies and does not alter the activity or mechanism of the peptide [17]. The F10W mutation exploits tryptophan's intrinsic fluorescence, which is evidently useful in fluorescence spectroscopy. In addition, to study effects of cationic residues, arginine and lysine, in peptide-DNA binding, mutants with all cationic residues modified to arginine or lysine,

referred to as all-arginine or all-lysine mutants respectively in this study, were designed using Swiss-PdbViewer.

2.2 Molecular Dynamics

Buforin II-DNA and DesHDAP1-DNA complexes were refined using MD simulations in Gromacs 4.5.5 using the AMBER-03 force field [17]. As mentioned before, the AMBER-03 force field was used due to its updated parameters for amino acids and nucleic acids. For all simulations, TIP4P-Ew waters were used, with Na^+ and Cl^- added to neutralize overall charges and provide an additional salt concentration of 100 mM, which is within the range of widely used salt concentrations to represent biological conditions [17, 24, 31]. Arginine and lysine residues and the N- and C- termini were ionized, while the single His side chain was left uncharged in the HID tautomer. Systems were then subjected to 100 steps of steepest descents minimization and heated to 298 K for 20 ps. Each MD trajectory was then extended to a total length of 50 ns at constant temperature (298 K) and isotropic constant pressure (1 bar). The scheme we used for simulation and computational analysis is shown below in Figure 6.

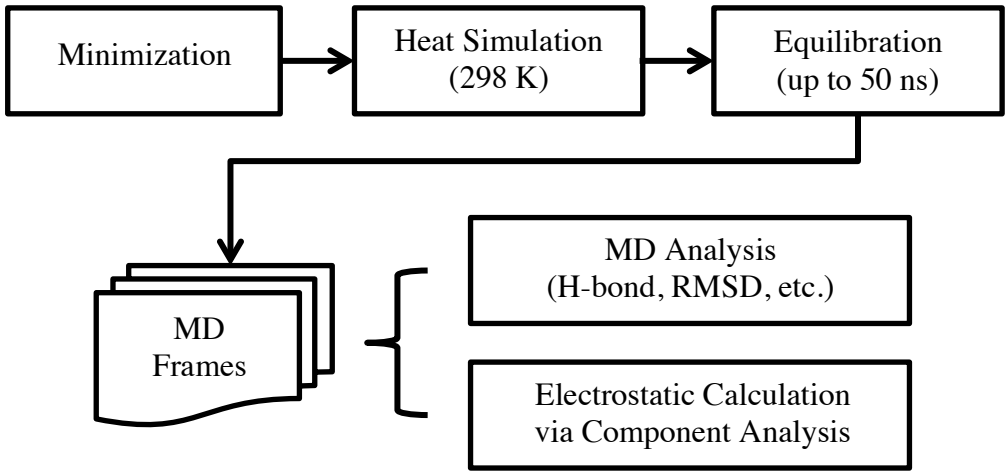

Figure 6. Simulation and analysis scheme used in this study.

All simulations used a time step of 2 femtoseconds, and long-range electrostatics longer than the 10-Å cutoff were calculated using PME. Bonds to hydrogen atoms were constrained using SHAKE [17]. For each type of peptide (i.e. buforin II, DesHDAP1, and their all-arginine and all-lysine mutants) bound to DNA, five simulations with identical initial structures were run and analyzed. For buforin II, of the five total simulations, three of them were extended to 100 ns, though these extensions appeared to show no qualitative differences in averaged properties in this study. MD analyses were then performed using tools in the GROMACS package.

2.3 Computational Analyses

2.3.1 RMS Deviation (RMSD)

Before analyzing from MD trajectories, it is important to confirm that the system of interest has equilibrated. Calculation of the root-mean-square deviation (RMS deviation) of atomic positions is a useful analysis to check for system equilibration and to investigate conformational changes.

$$RMSD = \sqrt{\frac{1}{N}\sum_{i=1}^{N} \|r_i(t) - r_i(0)\|^2}$$

Equation 6. Equation to compute the RMS deviation.

This analysis involves superimposing of the structure from every saved frame over a reference structure (often the initial structure). Then, the RMS deviation between these two structures is calculated. According to Equation 6, a major component of calculating the RMS deviation involves finding the difference between the distances of a selected atom *i*'s position at time *t* and the reference atom's position. For this study, the RMS deviations were calculated by fitting the DNA as well as fitting the Cα atoms of the structure of interest at time *t* and the initial structure.

Analysis of RMS deviation values helps validate the length of a simulation because when these deviation values start stabilizing, the system is not undergoing significant conformational changes. Therefore, in this study, different analyses were performed over the last 10 ns of simulations (40 ns to 50 ns period) as RMS deviation values stabilized from around 40 ns.

2.3.2 Hydrogen Bond Analysis

Hydrogen bonding is involved in interactions of many biomolecules, including DNA interactions of buforin II and DesHDAP1. The hydrogen bond analysis used in this study (gmx hbond in GROMACS) computes the number of hydrogen bonds formed between two selected groups at each saved frame and averages these numbers over a period of time. Thus, this analysis provided a simple and efficient way to estimate the interactions between the peptide and DNA.

2.3.3 Continuum Electrostatics Calculations and Component Analysis

Continuum electrostatic calculations were performed by solving the linearized Poisson Equation with a single-grid red-black successive over-relaxation finite-difference solver [29] for MD frames collected at every nanosecond from 40 ns to 50 ns. A dielectric constant of 4 was used for all peptide and DNA atoms, while the solvent was modeled using a dielectric constant of 80. Radii and charges of atoms were obtained from AMBER ff03 parameter files, in which radii depend only on element. A past study has also used AMBER parameters for electrostatic calculations [32]. A probe radius of 1.4 Å was used for defining the surfaces of these dielectric boundaries. Potentials were solved on a 301×301×301 grid. A two-tiered focusing procedure was used, with the peptide-DNA complex occupying 23% and 92% of the grid. Zero-radius and zero-charged dummy atoms were placed at identical minimum and maximum points of every

calculation for equal grid resolution. The grid spacing used yielded a resolution of approximately 2.92 grids per angstrom. Though this grids-per-angstrom value is relatively low, higher grid calculations were performed for a subset of grid calculations. Because no significant difference was observed in ΔΔG values for these higher grid calculations, results from the original grid calculations were considered and analyzed in this study. For these calculations, the ionic strength was set to 100 mM, which was the same value used in our MD simulations.

2.4 Visualization and Computational Details

Visual Molecular Dynamics (VMD) and PyMOL were used to generate images from simulations. Simulations and calculations were run with 3000 MHz AMD Opteron processors (from Wellesley College) and Intel Xeon Phi coprocessors (provided by XSEDE).

2.5 Fluorescent Intercalator Displacement (FID) Assay

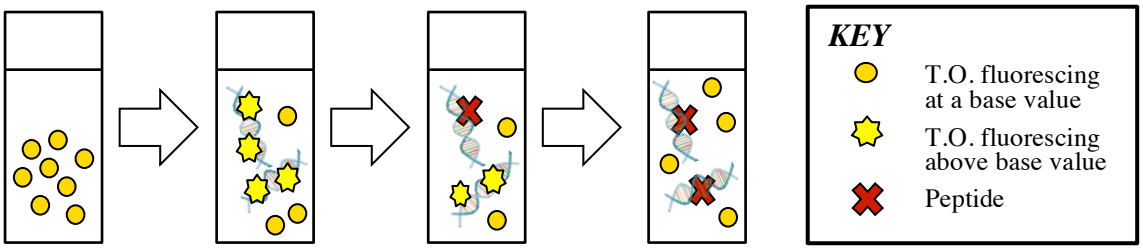

Figure 7. A FID assay scheme. After loading thiazole orange then nucleic acids into a cuvette, aliquots of a prepared peptide solution is added periodically followed by 5 minutes of incubation. As the peptide in the solution displaces the thiazole orange, the relative fluorescence decreases.

A fluorescent intercalator displacement (FID) assay (scheme shown in Figure 7) was used to experimentally measure relative DNA binding of each peptide and mutant [17]. Chemically synthesized wild type and mutant buforin II and DesHDAP1 at >95% purity were obtained from NeoScientific (Cambridge, MA) and GenScript (Piscataway, NJ). The double-stranded DNA for this experiment was obtained from ITC (Coralville, IA). To test for base selectivity in DNA

binding of buforin II and DesHDAP1, different repeating sequences of DNA (Table 4) were used to account for various possible combinations of sequences.

dsDNA name	Sequence
AC	ACA CAC ACA CAC ACA
CG	CGC GCG CGC GCG CGC
AG	AGA GAG AGA GAG AGA
AT	ATA TAT ATA TAT ATA

Table 4. Repeating sequences of dsDNA used in this study to test for base selectivity.

The FID assay, which has been used previously to measure relative DNA binding of HDAPs, involved loading of thiazole orange (0.55 μM), an intercalator that fluoresces upon binding double-stranded nucleic acids, in STE buffer (10 mM Tris, 50 mM NaCl, 1 mM EDTA, pH 8.0) into a quartz cuvette. Fluorescence was measured with 509 nm excitation and 527 nm emission and normalized to 0% relative fluorescence. Double-stranded DNA in STE buffer (1.1 μM of base pairs) was then added. The solution was equilibrated for 5 minutes followed by measurement of fluorescence normalized to 100% relative fluorescence. Aliquots of a prepared peptide solution (7.8×10^{-5} M) were added periodically before mixing, with five minutes of incubation before subsequent measurements of fluorescence. Concentration of peptide required to reduce fluorescence, as peptides displaced thiazole orange bound to DNA, to half its initial value, or C_{50}, was determined by a linear curve fit, as shown in Figure 8. All fits for data included in averaging had $R^2 > 0.88$. The relative DNA binding constants were expressed as the reciprocal of C_{50}, or $1/C_{50}$. Thus, a greater $1/C_{50}$ implies more favorable binding as less peptide is required to reach the half fluorescence point. For each dsDNA, binding constants for both buforin II and DesHDAP1 were measured in at least seven independent experiments.

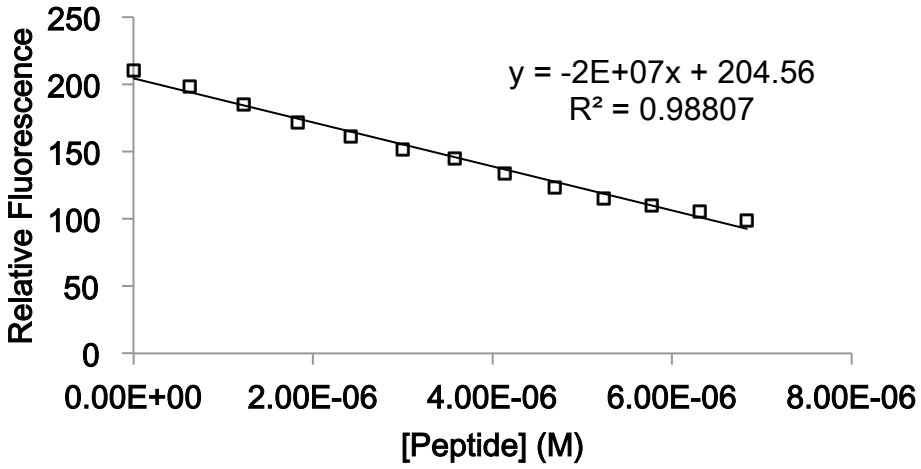

Figure 8. A sample FID assay experiment. Note that the relative fluorescence decreases as the concentration of peptide in solution increases. After the relative fluorescence drops below half of the initial fluorescence value, C_{50} is determined by a linear curve fit.

3. Results and Discussion

3.1 Structural Sampling via MD Simulations

Due to the structural complexity of the histone H2A protein, the sections corresponding to sequences of buforin II and DesHDAP1 after isolation likely do not represent the natural conformations of their free peptide counterparts. Therefore, subjecting these structures to MD simulations allows them to explore potential peptide conformations and binding orientations.

To quantify the conformational changes in binding orientations of a peptide, the RMS deviation from its initial conformation was computed by superimposing the DNA backbone throughout the trajectory. By essentially holding down the position of the DNA backbone, relative changes in binding positions on the DNA were observed, as shown in Figure 9. Though the dsDNA in each simulation also changed its conformation, these changes were not as significant.

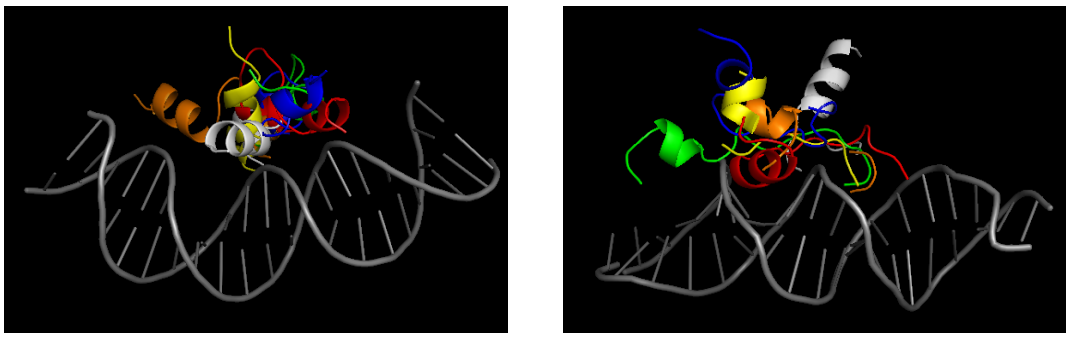

Figure 9. Changes in binding positions of buforin II (left) and DesHDAP1 (right) on DNA (dsDNA from initial structures of peptide-DNA complexes). The initial positions are shown in white. The non-white structures are final binding positions (at 50 ns) from five independent simulations after superimposing the DNA backbone.

On the other hand, to observe changes in the peptide structure, the RMS deviation was computed again but this time by superimposing or fitting the Cα atoms throughout the trajectory. Below are initial conformations of buforin II (shown on the left) and DesHDAP1 (shown on the right) before subjecting them to MD simulations:

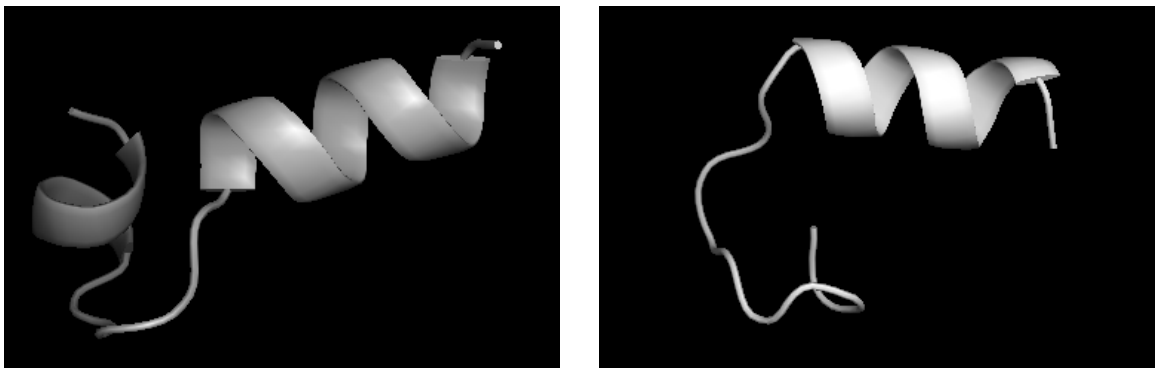

After subjecting these initial structures to MD simulations, changes in peptide conformations were evident. The final structures of buforin II taken from the 50 ns frame of each of the five total simulations have been superimposed to the initial structure to visualize the changes in buforin II's conformation:

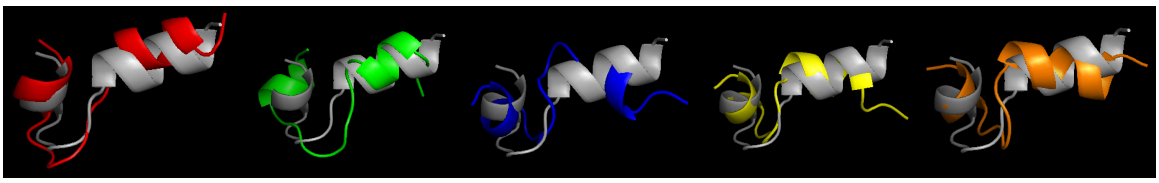

The same has been done for DesHDAP1, using the initial structure as reference, to note the changes in its conformation:

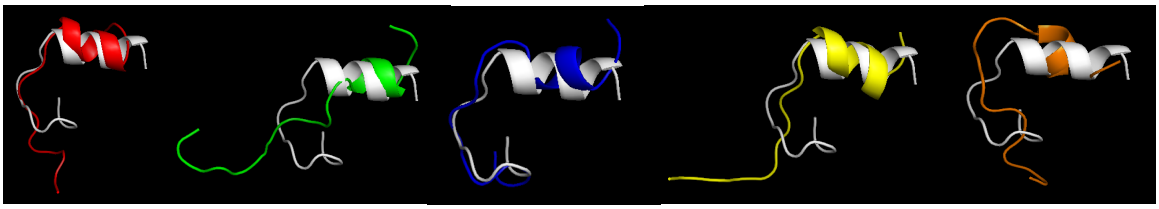

The series of snapshots not only provided visual representations of the RMS deviations with respect to the initial structure but also helped justify our use of MD to explore potential peptide conformations and binding positions as we can see that both peptides changed their conformations and positions significantly throughout the trajectories.

3.2 System Equilibration

Before performing computational analyses on sets of frames from our MD simulations, the RMS deviations fitting DNA and Cα atoms were computed for each simulation to check for system equilibration. Generally, the length of a simulation is considered sufficient if it contains frames in which the RMS deviations stabilize, i.e. contains frames that suggest there is systematic irreversible movement toward some equilibrium state. For our peptide-DNA systems,

we wanted to check that in our simulations, both the RMS deviations fitting the DNA and the Cα atoms stabilized by the end.

3.2.1 Structural Equilibration and Sampling of Buforin II

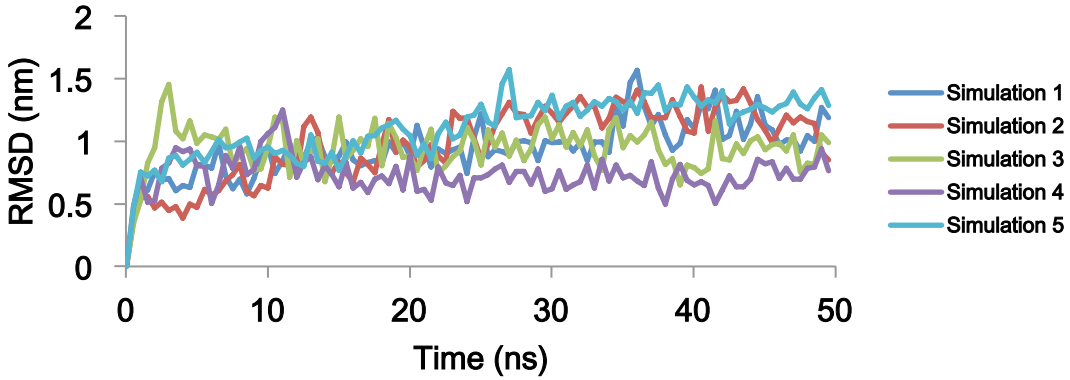

Figure 10. A plot of DNA-fitted RMSD vs. time for five simulations of buforin II bound to DNA.

According to the Figure 10, all five simulations of buforin II appear to have reached an equilibrated conformation of the peptide with respect to DNA, particularly during the last ten-nanosecond periods as the RMS deviations stabilize about a constant value. This is more evident in the figure below, in which we zoom into the last ten-nanosecond period of the simulation.

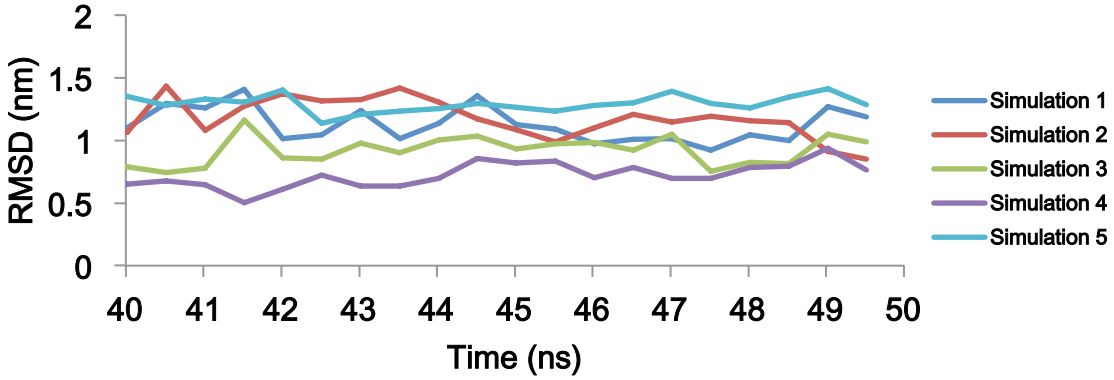

Figure 11. A plot of DNA-fitted RMSD vs. time (40 - 50 ns) for simulations of buforin II.

In addition, the peptide conformation also appeared to have stabilized in this 40 to 50 ns period for buforin II, as observed in Figure 12.

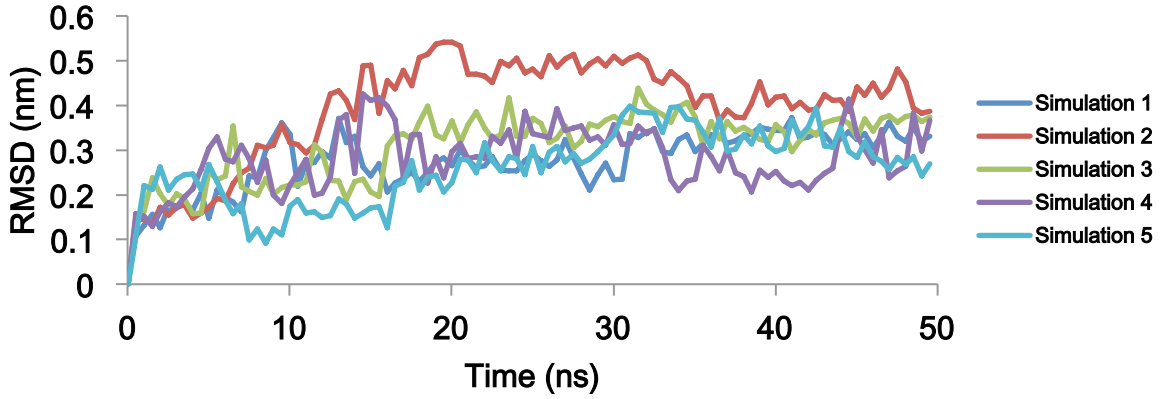

Figure 12. A plot of Cα-fitted RMSD vs. time for five simulations of buforin II bound to DNA.

Again, we zoomed into the last ten nanoseconds of the simulation to highlight the equilibrated region:

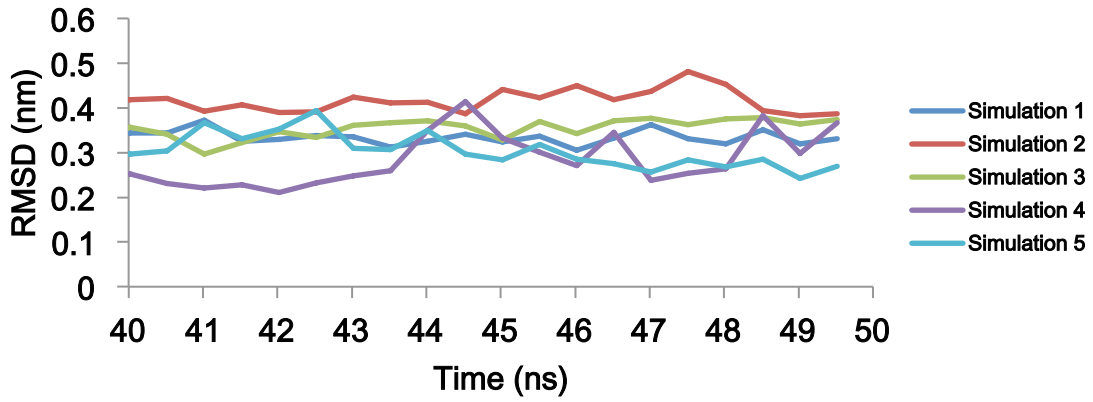

Figure 13. A plot of Cα-fitted RMSD vs. time (40 - 50 ns) for simulations of buforin II.

From the scale of this figure, we observe that in each simulation, buforin II maintains its conformation towards the end of simulations. However, from a previous figure, Figure 9, we noted that the final structures of buforin II from each of the five simulations varied relative to the initial structure and to each other in both the DNA and Cα-fitted cases. That is, generally, the conformational changes primarily increased the interactions between the helical region and the DNA backbone, shown in Figure 14, though the positions assumed by helices to increase interactions with DNA in these simulations were not identical.

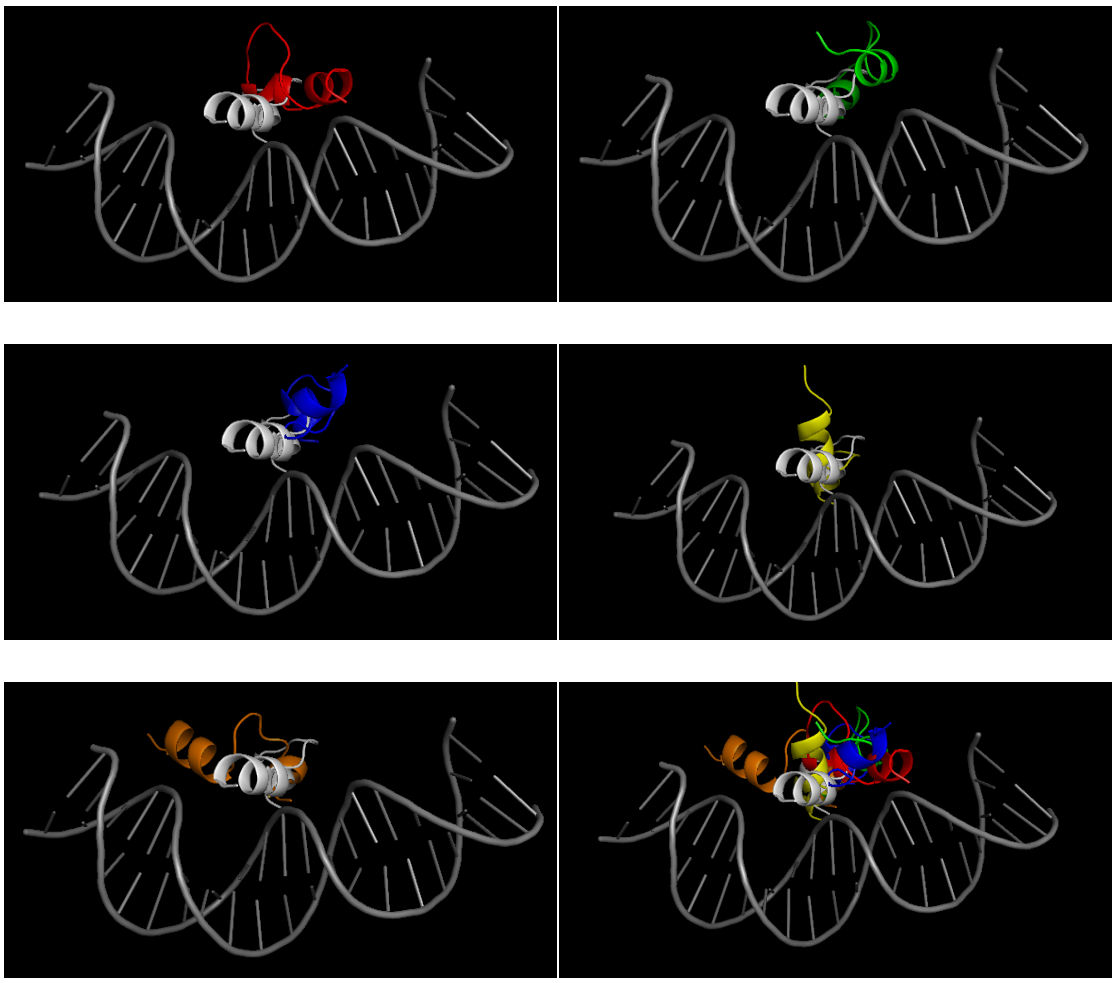

Figure 14. Various conformations of buforin II relative to DNA (dsDNA from the initial structure of buforin II-DNA complex). Initial structure shown in white. Note the increased the interactions between the helical region and the DNA backbone.

3.2.2 Structural Equilibration and Sampling of DesHDAP1

Similar to buforin II, DesHDAP1 peptides were also shown to have explored a range of peptide conformations relative to DNA in all simulations. All five simulations of DesHDAP1 appeared to have reached equilibrated conformations near the last ten nanoseconds of simulations, shown by the RMSD plots below:

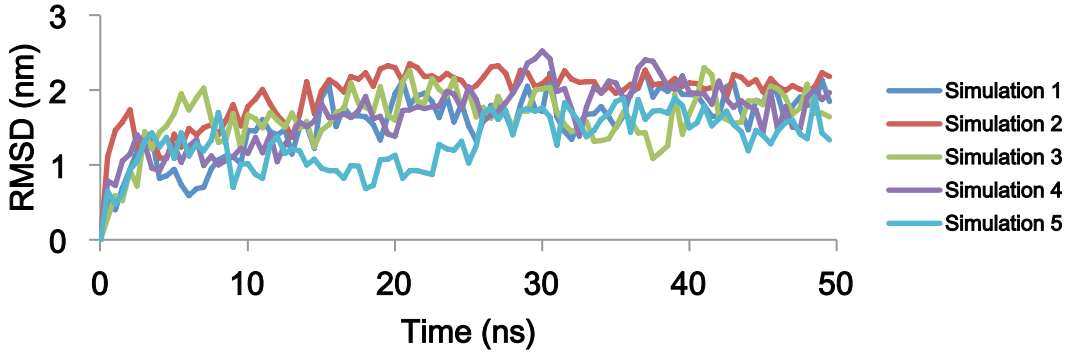

Figure 15. A plot of DNA-fitted RMSD vs. time for five simulations of DesHDAP1 bound to DNA.

We again zoomed into the last ten nanoseconds to check for equilibration:

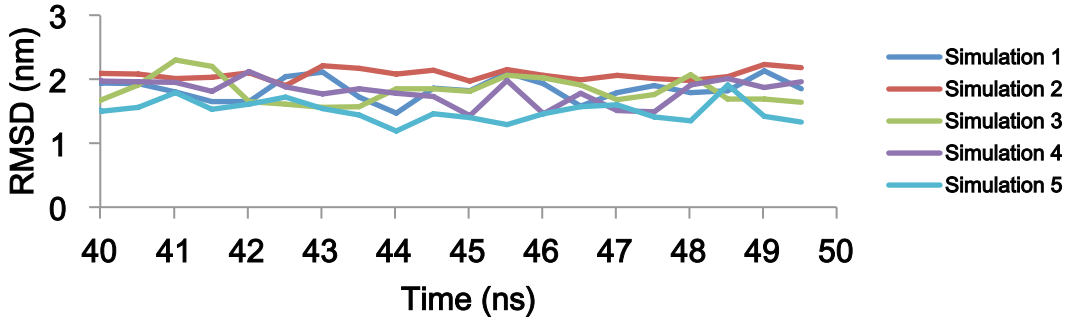

As was with buforin II, simulations of DesHDAP1 maintained peptide conformations relative to the DNA, a good indication that the system has equilibrated.

The RMS deviations of peptide conformations relative to the initial structure were also computed, as shown in Figure 16.

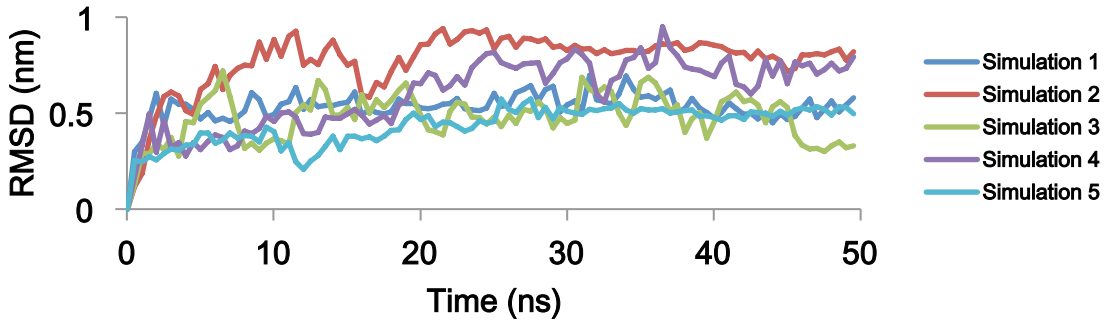

Figure 16. A plot of Cα-fitted RMSD vs. time for five simulations of DesHDAP1 bound to DNA.

Figure 16 as well as the zoomed-in Figure 17 showed that the DesHDAP1-DNA complexes have equilibrated.

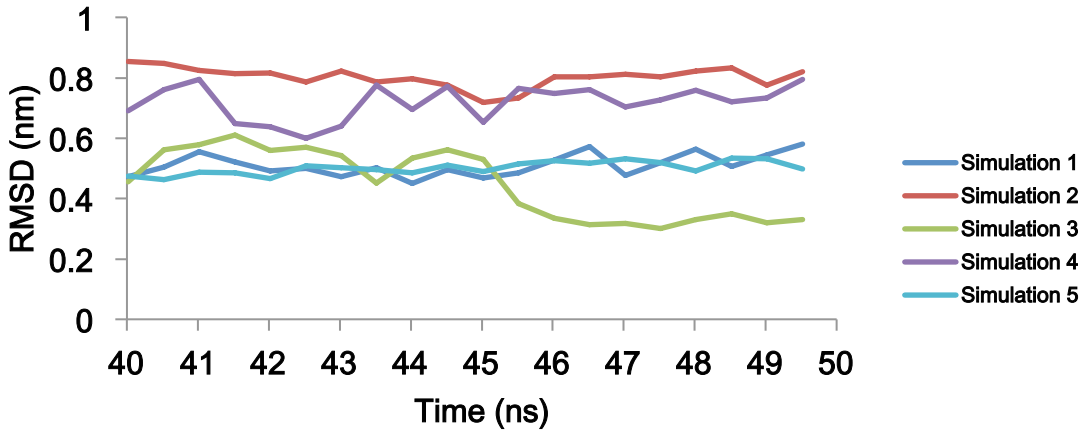

Figure 17. A plot of Cα-fitted RMSD vs. time (40 - 50 ns) for simulations of DesHDAP1.

In addition to noting conformational changes by calculating RMS deviations, snapshots from simulations of DesHDAP1 showed that while DesHDAP1's terminal portions were positioned relatively far from the DNA backbone in the histone-based initial structure, all simulations adjusted the system to create additional peptide-DNA contacts, as shown below:

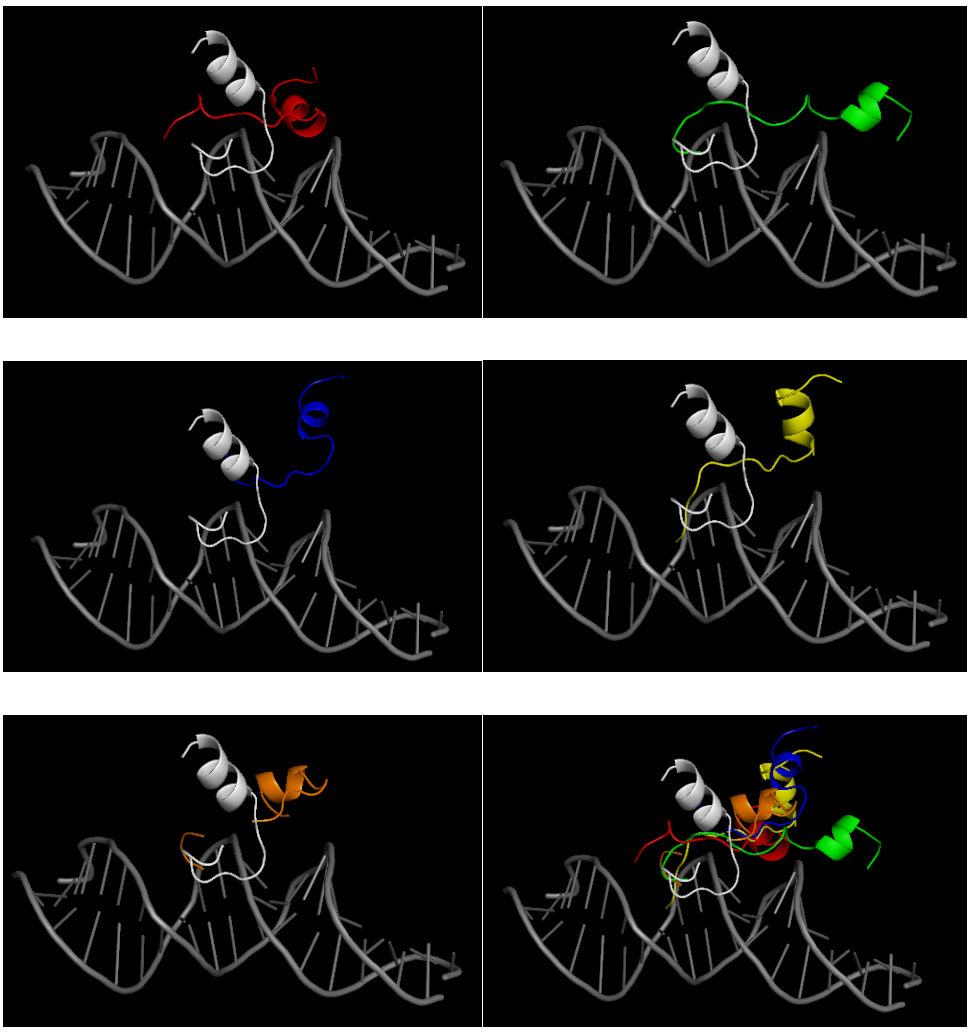

Figure 18. Various conformations of DesHDAP1 relative to DNA (dsDNA from the initial structure of DesHDAP1-DNA complex). Initial structure shown in white.

This was reasonable considering the concentration of positive charges in that region of the peptide. Four of the simulations placed the N-terminal region in the same major groove, with the other simulation (simulation 3 shown in blue) showing the peptide diffusing to an adjacent region of DNA. While the C-terminal helix region generally did move towards the peptide, this was less consistent between simulations.

3.3 RMSD Results

It was impossible to evaluate the "true" structure of the buforin II-DNA or DesHDAP1-DNA complex as we observed a range of potential conformations from our simulations. In fact, it is more likely that the actual bound systems may assume a variety of different orientations, which was supported by our RMSD results. However, though the RMS deviations of our simulations for both buforin II and DesHDAP1 converged at different values, each simulation in a set shared several similarities in trends regarding peptide-DNA binding with the other four. And these similarities gave us increased confidence that our selectivity predictions were not biased by considering one potential conformation.

3.4 Length of Simulations

To increase our sampling in conformations, we extended three simulations of buforin II to 100 ns. Results from these extended simulations did not have significant changes in averaged properties used for analyses of buforin II-DNA binding. For example, Figure 19 shows that the average number of hydrogen bonds formed between buforin II and the DNA per time frame for 50 ns simulations and 100 ns simulations are not significantly different.

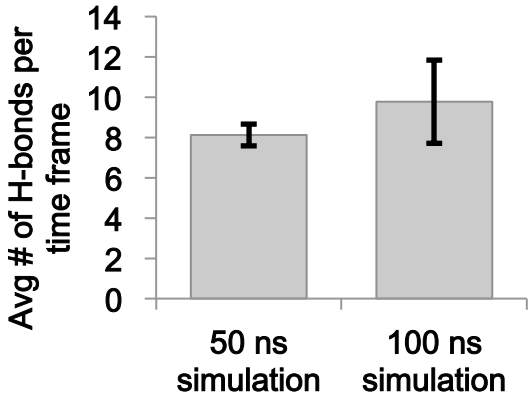

Figure 19. Average number of H-bonds per time frame for 50 ns and 100 ns simulations of buforin II.

Therefore, 50 ns simulations appeared to be sufficient in length, at least for our systems, in which we performed analyses over the last 10 ns of these 50 ns simulations. However, for a more thorough analysis on lengths of simulations, we may also extend simulations of DesHDAP1 to 100 ns to check that there are no significant changes in averaged properties.

3.5 Base Selectivity

3.5.1 Computational Analyses on Base Selectivity

According to previous work, buforin II peptides were predicted to interact primarily with the phosphate groups of the DNA backbone. By extending the study to include DesHDAP1 and employing various analyses to quantify DNA interactions, we were able to support past results. The first analysis used to quantify DNA interactions of buforin II and DesHDAP1 involved computing the percentage of hydrogen bonds formed between a peptide and DNA. While the raw numbers of hydrogen bonds between a peptide and DNA fluctuated among the five simulations for each peptide, a significant percentage of the bonds involved phosphate groups in all simulations. For example, no simulation of buforin II had less than 86.8% of peptide-DNA H-bonds involving phosphates, and no DesHDAP1 simulation had less than 66.8% of peptide-DNA

H-bonds with phosphate groups (Table 5). Because these phosphate groups are identical for any nucleic acid sequence, these results imply that there is likely little to no selectivity for particular DNA sequences [33, 34]. Interestingly, there was no clear correlation between the extent of conformational change observed over the course of a simulation and significantly increased or decreased DNA interactions. As an example, we observed noticeable conformational changes among simulations of DesHDAP1 relative to the DNA yet the percentages of hydrogen bonds with the phosphate groups were still significant.

	BF2	**Des1**
Simulations	% H-bonds to phosphate	% H-bonds to phosphate
1	98.9	72.2
2	86.8	86.3
3	98.1	94.6
4	100	66.8
5	100	84.0
Average ± SE	96.8 ± 2.5	80.8 ± 5.0

Figure 5. Interaction results from MD simulations of buforin II and DesHDAP1 with DNA. H-bonding data reports the average percentages of all peptide-DNA hydrogen bonds that involved the nucleic acid phosphate groups. All values averaged over structures taken from the last 10 ns of simulations.

To provide an energetic consideration of the peptide-DNA interactions, electrostatic calculations were used to quantify average peptide-DNA interactions from frames collected over the last 10 ns of simulations. To consider the portion of overall interactions involving phosphate groups, we calculated the ratio, $\Delta\Delta G_{phos}$:$\Delta\Delta G_{bases}$ (Table 6). $\Delta\Delta G_{phos}$ is essentially the contribution of peptide-phosphate group interaction to the overall electrostatic binding energy between the peptide and DNA. Similarly, $\Delta\Delta G_{bases}$ is the contribution of peptide-base interaction. The ratios found for the simulations, which are greater than 1, further support that the primary interactions between both peptides and DNA involve phosphate groups.

	BF2	Des1
Simulations	$\Delta\Delta G_{phos}$:$\Delta\Delta G_{bases}$	$\Delta\Delta G_{phos}$:$\Delta\Delta G_{bases}$
1	11.5	7.3
2	8.2	5.6
3	23.7	6.4
4	20.1	3.0
5	21.8	5.5
Average ± SE	17.1 ± 3.0	5.6 ± 0.69

Table 6. Interaction results from MD simulations of buforin II and DesHDAP1 with DNA. $\Delta\Delta G_{phos}$:$\Delta\Delta G_{bases}$ is the ratio of the free energy involving the phosphate groups compared to other atoms in the nucleic acid bases as determined from electrostatic calculations. All values averaged over structures taken from the last 10 ns of simulations.

Buforin II	**1**	**2**	**3**	**4**	**5**	**Average ± SE**
$\mathbf{\Delta\Delta G_{phos}}$ (kcal/mol)	-43.3	-46.5	-51.2	-52.8	-46.6	-48.1 ± 1.7
$\mathbf{\Delta\Delta G_{bases}}$(kcal/mol)	-3.8	-5.6	-2.2	-2.6	-2.1	-3.3 ± 0.7
$\mathbf{\Delta\Delta G_{phos+ribose}}$ (kcal/mol)	-23.3	-23.4	-27.1	-28.6	-27.5	-26.0 ± 1.1

DesHDAP1	**1**	**2**	**3**	**4**	**5**	**Average ± SE**
$\mathbf{\Delta\Delta G_{phos}}$ (kcal/mol)	-27.7	-35.4	-19.3	-26.0	-40.4	-29.7 ± 3.7
$\mathbf{\Delta\Delta G_{bases}}$(kcal/mol)	-3.8	-6.3	-3.0	-8.6	-7.3	-5.8 ± 1.0
$\mathbf{\Delta\Delta G_{phos+ribose}}$ (kcal/mol)	-12.6	-16.1	-8.2	-11.1	-19.4	-13.5 ± 1.9

Table 7. Raw ΔΔG values referring to contributions of the phosphates, bases, and a combination of phosphate and ribose groups.

Raw ΔΔG values were also provided in Table 7 as another way to note the difference in contributions of the DNA phosphates and bases to the overall electrostatic binding free energy. Interestingly, by zeroing charges of both the phosphate and ribose groups, the corresponding ΔΔG values increased. This may be due to the fact that though ribose groups are also part of the DNA backbone, they contribute unfavorably to the binding energy. Thus, to confirm this hypothesis, calculating $\Delta\Delta G_{ribose}$ could be a next potential step.

To directly test for base selectivity using simulations, we modeled peptide-DNA systems containing the repeating DNA sequences from Table 4. For buforin II, we ran four 50 ns

simulations, in which each simulation contained one of the four repeating DNA sequences. We then repeated the procedure for DesHDAP1. From our previous simulations of buforin II and DesHDAP1 bound to the adjacent dsDNA, we had observed that the raw numbers of H-bonds between a peptide and DNA fluctuated. Thus, we expected raw numbers for these simulations to fluctuate as well, especially considering the fact that we only ran one simulation per repeating sequence and could not average any results. This also highlights the fact that while computing the number of H-bonds may provide insight and general trends in DNA binding, it certainly is not a direct substitution for calculating binding free energies. Therefore, we calculated the percentage of H-bonds formed between the peptide and DNA (Table 8).

	BF2	**Des1**
Repeating Sequence in Simulation	% H-bonds to phosphate	% H-bonds to phosphate
AC	99	86
AG	98	72
AT	100	92
CG	100	74

Table 8. H-Bonding data from simulations of buforin II and DesHDAP1 with repeating DNA sequences. All values averaged over structures taken from the last 10 ns of simulations.

As expected, a significant percentage of the bonds involved phosphate groups in all simulations shown in Table 8. In addition, comparing percentage values of buforin II and DesHDAP1, values for DesHDAP1 were generally less than values for buforin II, which was consistent with our H-bonding results from Table 5. Thus, this analysis further supported our hypothesis that the DNA binding of buforin II and DesHDAP1 had little to no selectivity in base sequence.

3.5.2 Experimental Binding Measurement for Base Selectivity

Our computational analyses suggested that little to no selectivity in base sequence should be expected for buforin II and DesHDAP1 binding of DNA, as both peptides interact primarily with the phosphate groups of nucleic acids. To experimentally test this observation, a fluorescent intercalator displacement (FID) assay was used to measure relative binding constants of buforin II and DesHDAP1 bound to one of four different double-stranded DNA sequences (Table 4). The $1/C_{50}$, which is proportional to the binding constant, was compared for the peptides with each DNA strand (Figure 20). The uncertainty $1/C_{50}$ measurements were overlapping for binding with different base sequences, and no significant differences arose in one-way ANOVA analyses of these results. Thus, these experiments appear to confirm the predicted lack of sequence specificity in the DNA binding for these two peptides.

(A)

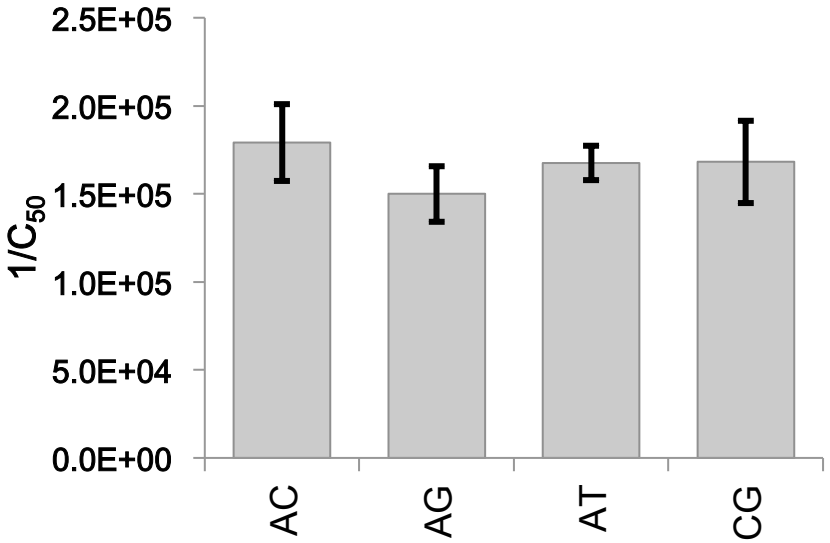

(B)

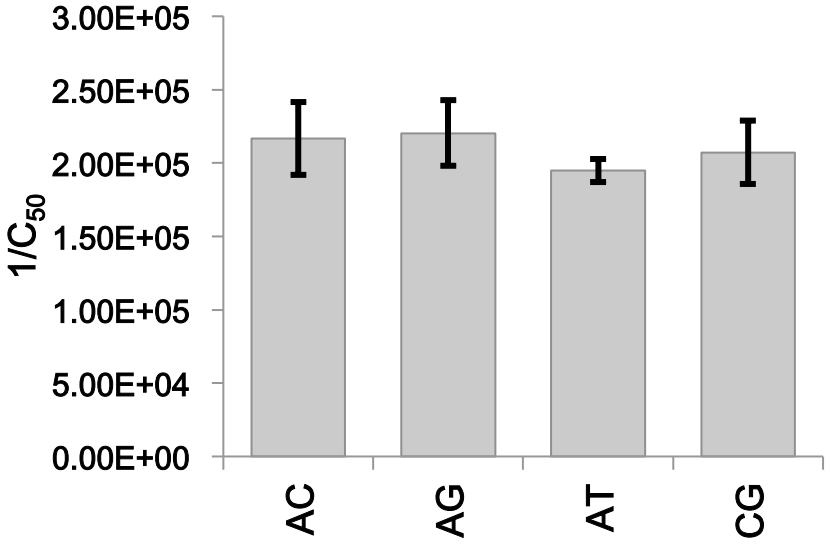

Figure 20. Experimentally measured relative binding constants, expressed as 1/C50, for buforin II (A) and DesHDAP1(B) with different double-stranded DNA sequences, as given in Table 4. All data reported is averaged from at least seven independent binding experiments with error bars shown as standard error.

In addition to the phosphate interactions, we also noted an interesting trend when considering which peptide residues were primarily involved in mediating interactions with DNA. Previous work has investigated roles of cationic residues, arginine and lysine, in translocation and

antimicrobial activity of various HDAPs including buforin II and DesHDAP1 [35]. According to this study, higher arginine content appeared to increase translocation for both buforin II and DesHDAP1. Interestingly, they noted that while the wild type buforin II and all-arginine mutant of buforin II exhibited comparable relative translocating abilities, there was an increased antimicrobial activity observed for the all-arginine mutant. This led to a hypothesis that this increased activity of the all-arginine mutant may have resulted from altered binding to its intracellular target, which is believed to be nucleic acids in the cases of buforin II and DesHDAP1. Thus, simulations of all-arginine and all-lysine mutants were run to investigate the effects of arginine and lysine in DNA binding of buforin II and DesHDAP1.

3.6 Arginine vs. Lysine in DNA Binding

3.6.1 Computational Analyses on Role of Arginine

For both computational and experimental analyses to investigate effects of having cationic residues in peptide composition that are arginine instead of lysine, all-arginine and all-lysine mutants of buforin II and DesHDAP1 were modeled (Table 7).

Peptide Name	**Sequence**
Buforin II R (BF2R)	TRSSRAGLQWPVGRVHRLLR**R**
Buforin II K (BF2K)	T**K**SS**K**AGLQWPVG**K**VH**K**LL**K**K
DesHDAP1 R (Des1R)	ARDN**RR**TRIWPRHLQLAVRN
DesHDAP1 K (Des1K)	A**K**DNKKT**K**IWP**K**HLQLAV**K**N

Table 9. Sequences of all-arginine and all-lysine mutants of buforin II and DesHDAP1.

When referring to an all-arginine mutant, this corresponds to a peptide in which all lysine residues in the original peptide composition has been mutated to arginine. Similarly, an all-lysine mutant has had all its original arginine residues mutated to lysine.

As one might expect, when subjected to the hydrogen bond analysis, the cationic arginine and lysine residues formed the majority of H-bond interactions with DNA in each simulation (Figure 21).

(A)

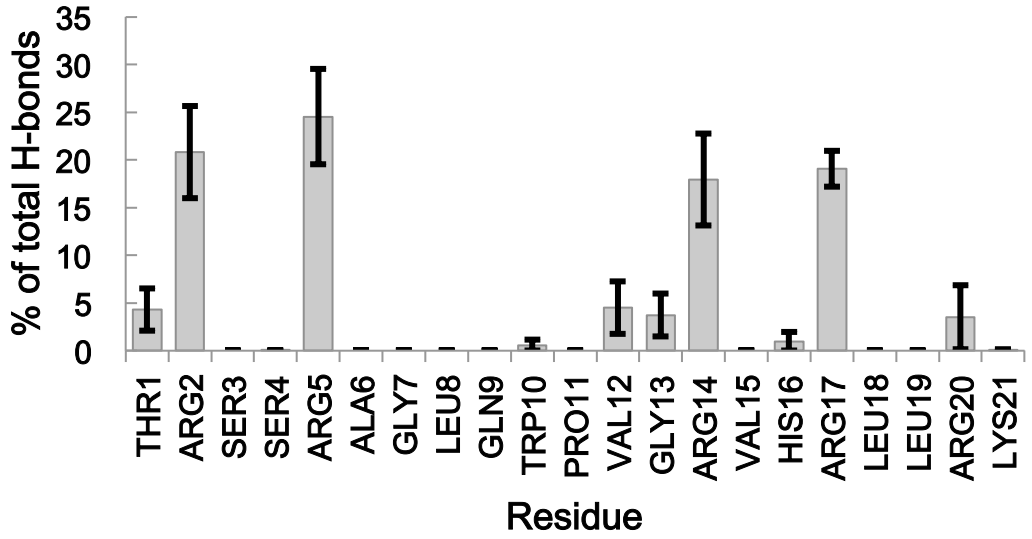

(B)

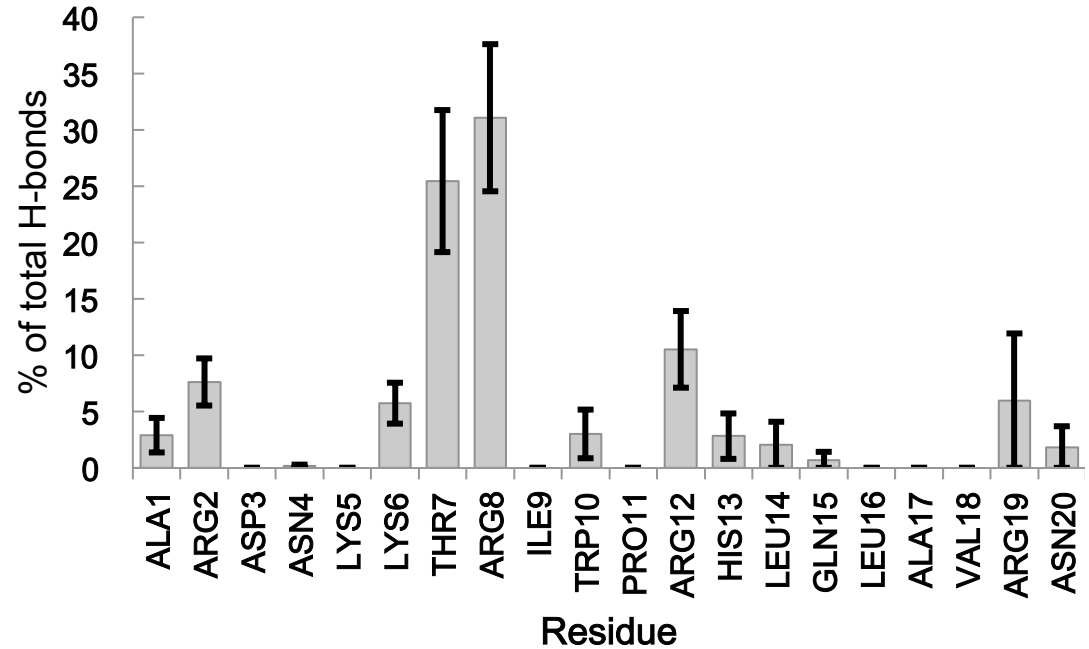

Figure 21. Average percentage of total peptide-DNA H-bonds involving each peptide residue in simulations of buforin II (A) and DesHDAP1 (B). Percentages for each simulation determined over the last 10 ns, with the error bars shown as the standard error from averaging values from the five simulations.

According to Figure 21, the only neutral residue that formed DNA interactions in all simulations for either peptide was the Thr 7 residue of DesHDAP1, which is flanked on either side by cationic residues. However, within cationic residues, arginine residues form notably more DNA interactions than lysine residues, with arginine forming over 90% of the cationic residue-DNA H-bonds in both buforin II and DesHDAP1 simulations. While arginine residues are more prevalent in wild types of these peptides, they are nonetheless overrepresented relative to lysine in terms of direct interactions with DNA. This may be due to the ability of the guanidinium group in arginine sidechains to form bidentate interactions with the DNA phosphate groups, which cannot occur for the primary amine in lysine [11, 25, 36] (Figure 22).

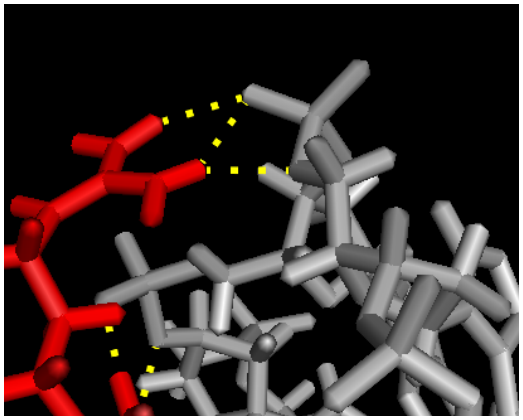

Figure 22. Arginine of buforin II (red) forming bidentate interactions with the DNA phosphate group (gray).

Following our H-Bond analysis that focused on each arginine and lysine residue in buforin II and DesHDAP1, we performed a similar residue-by-residue analysis using continuum electrostatic calculations and obtained similar trends (Figure 23).

(A)

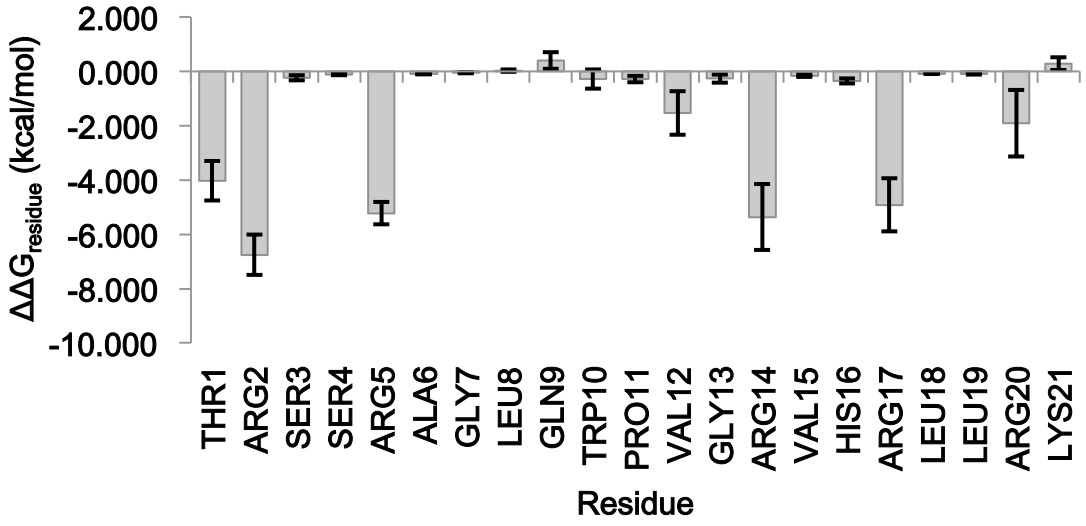

(B)

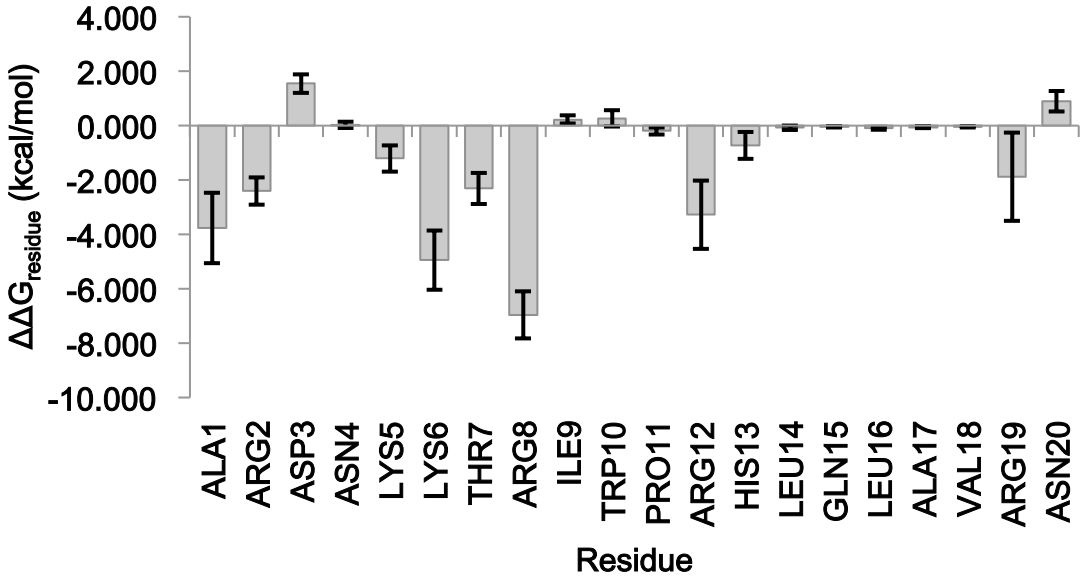

Figure 23. Average ΔΔG of each residue in (A) buforin II and (B) DesHDAP1. Average for each simulation determined over the last 10 ns, with the error bars shown as the standard error from averaging values from the five simulations.

Again, we observed that arginine residues generally contributed more to the electrostatic binding free energy than lysine residues.

Another H-bond analysis was then performed but this time to directly compare the averaged DNA interactions of all-arginine vs. all-lysine mutants. All-arginine mutants for both buforin II and DesHDAP1 were shown to have greater average numbers of H-bonds per time frame compared to their lysine mutant counterparts (Figure 24), suggesting that having a large arginine content in the peptide structure increases the peptide-DNA interaction.

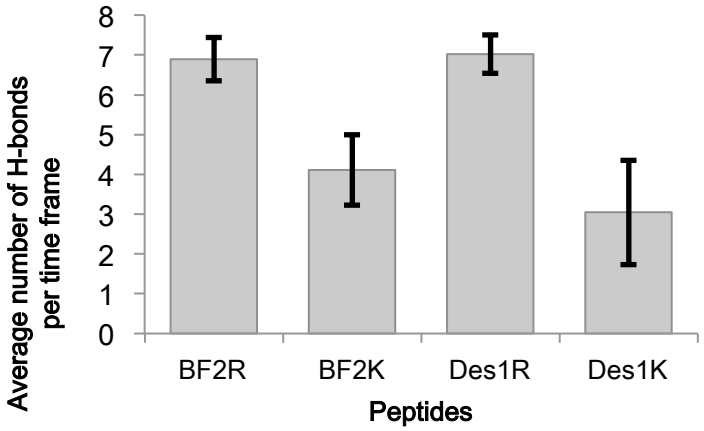

Figure 24. Average number of H-Bonds formed between peptide and DNA. All-arginine mutants for both buforin II and DesHDAP1 formed greater interactions with the DNA. Average for each simulation determined over the last 10 ns, with the error bars shown as the standard error from averaging values from the five simulations.

To verify our results from both H-bond analyses, the electrostatic components of the binding energies, or ΔG_{elec}, of all-arginine and all-lysine mutants of buforin II and DesHDAP1 were determined as shown in Figure 25.

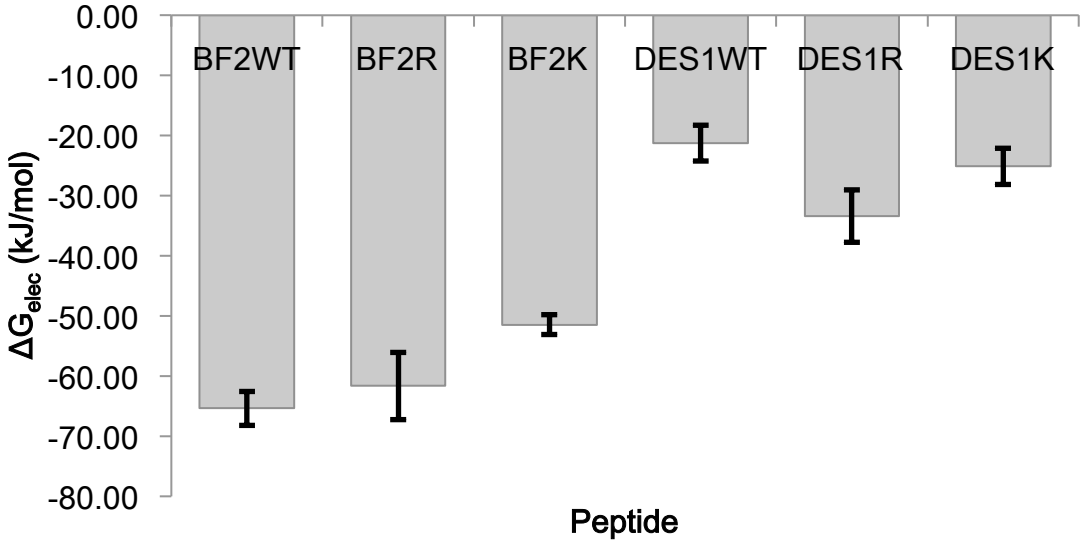

Figure 25. Electrostatic components of binding free energies of all-arginine and all-lysine mutants of buforin II and DesHDAP1.

Indeed, the electrostatic component of binding energies of arginine mutants of both buforin II and DesHDAP1 appeared more energetically favorable, confirming our H-bond analyses. Therefore, from past studies and our various computational analyses, having increased arginine content in peptide composition appeared to improve translocation as well as DNA binding.

3.6.2 Experimental Studies in Role of Arginine

As was done to verify computational data on base selectivity, the FID assay was used again to verify our predictions on the role of arginine in buforin II's and DesHDAP1's antimicrobial activity. After obtaining all-arginine and all-lysine mutants of buforin II and DesHDAP1, relative binding constants were collected, as shown in Figure 26:

(A)

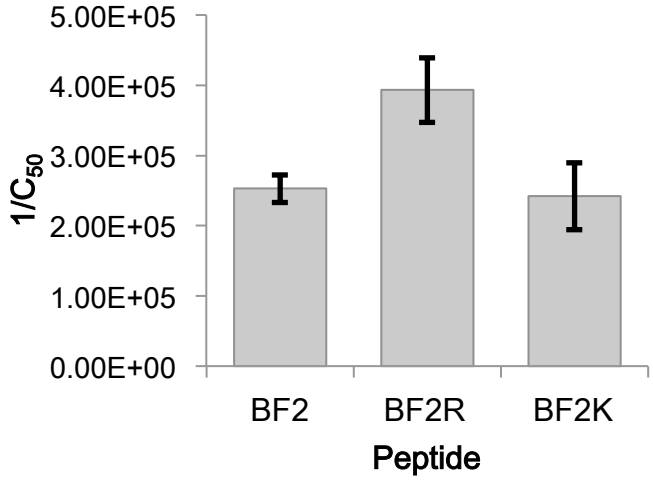

(B)

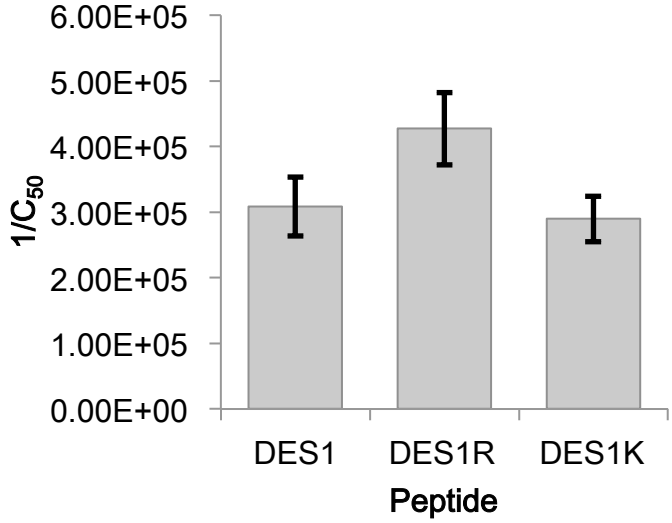

Figure 26. Experimentally measured relative binding constants, expressed as $1/C_{50}$, for (A) buforin II and (B) DesHDAP1 mutants. All data reported is averaged from at least seven independent binding experiments with error bars shown as standard error.

For both buforin II and DesHDAP1, the all-arginine mutants had more favorable DNA interactions, confirming our computational results. However, even though our experimental data for all-arginine and all-lysine mutants appeared to correspond to computational data, the

experimental and computational results for wild type peptides were not consistent. For example, in the H-bond results for buforin II and its mutants (Figure 27), simulations containing the wild type peptide and the all-arginine mutant showed comparable average numbers of H-bonds formed between the peptide and DNA.

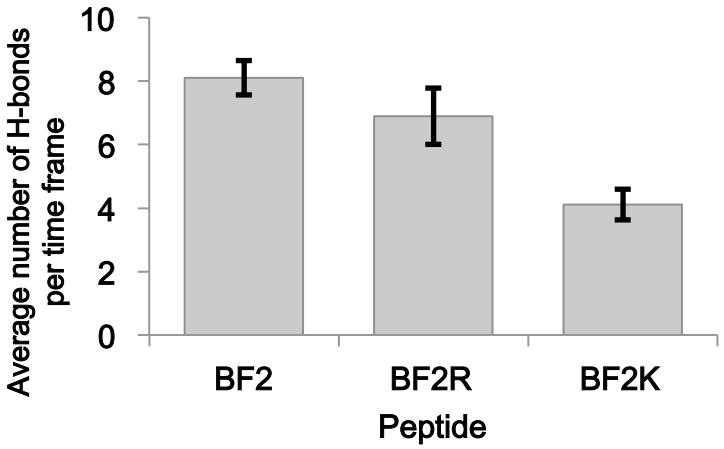

Figure 27. Average number of H-Bonds formed between peptide and DNA for buforin II (wild type) and its mutants.

Figure 26, however, showed that the all-arginine buforin II mutant had significantly more favorable interactions with DNA compared to the DNA interactions of the wild type. These relative binding constants shown in Figure 26 were collected by three individuals, and it is possible that our experimental data is not representative of what is observed in reality. That is, our $1/C_{50}$ values for the all-arginine mutants appeared too high in value. To check for accuracy, we checked both our computational and experimental data. When I started collecting preliminary data for the relative binding constants for buforin II and its mutants, it was noted that the $1/C_{50}$ values from my experiments better corresponded to our computational data (Figure 25 and 28). In both data sets, there did not appear to be significant differences in DNA binding for buforin II

wild type and its all-arginine mutant. However, it is necessary to collect more data points for relative binding constants for buforin II, DesHDAP1, and their mutants.

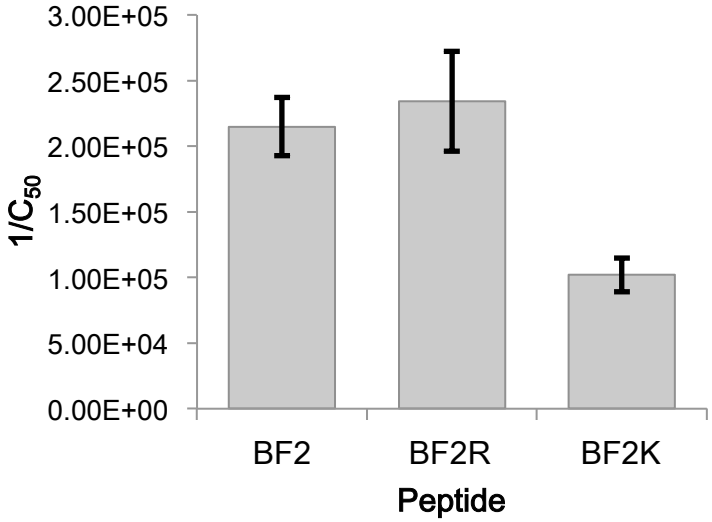

Figure 28. Preliminary relative binding constant results for buforin II and its mutants. Though incomplete, this set of experimental data better corresponds to computational data.

4. Conclusion

In this study, the DNA binding of two HDAPs, buforin II and DesHDAP1, was characterized using a combination of computational and experimental methods. While many antimicrobial peptides were shown to kill pathogens mainly through membrane permeabilization, AMPs with alternative mechanisms of action are currently being discovered and better characterized for possible therapeutic applications. Therefore, a thorough study and understanding of AMPs and their mechanisms of action are necessary.

Our use of MD was crucial to the study as simulations of buforin II and DesHDAP1 allowed for initial structures extracted from the histone protein to equilibrate and explore

potential conformations. Though the final conformations and positions of peptides from each simulation in a set were different, they still provided comparable trends such as showing significant interactions with the DNA phosphates. While the differences in final structures did not lead to any conclusive structures of buforin II-DNA or DesHDAP1-DNA complex, the fact that these different simulations still led to comparable results in base selectivity gave us confidence that our results were reasonable and unbiased.

Then, taking advantage of computational methods and their abilities to focus on the system of interest at the molecular level, we were able to show that the DNA binding of buforin II and DesHDAP1 is not base selective. Specifically, both buforin II and DesHDAP1 interact primarily with the phosphates of the DNA backbone, which are identical for any nucleic acid sequences. Using an experimental method, we were then able to confirm our prediction.

Previous work on DNA binding of HDAPs also focused on the role of cationic residues, arginine and lysine. By implementing the computational and experimental methods that we have used before to prove the lack of base selectivity in DNA binding, we were able to show that having cationic residues that are arginine instead of lysine generally led to enhanced DNA binding. This was at least partly due to arginine's ability to form bidentate interactions with the DNA.

Though this study provided a more comprehensive characterization of DNA binding of buforin II and DesHDAP1 using systematic use of computational and experimental methods, there is still work to be done to further this study. For example, by our reasoning that the lack of base selectivity is due to significant interactions with phosphates, nucleic acid binding of buforin II and DesHDAP1 is likely not base selective. In fact, we ran a 50 ns simulation for buforin II bound to repeating sequences of AU (AUA UAU AUA UAU AUA) and repeated the procedure

for DesHDAP1. When we calculated the percentages of H-bonds to phosphates of the RNA backbone (Table 10), these percentages were comparable to those we obtained for peptides bound to repeating DNA sequences, which was shown in Table 8.

	BF2	**Des1**
Repeating Sequence in Simulation	% H-bonds to phosphate	% H-bonds to phosphate
AU	100	92

Table 10. Preliminary H-Bonding data from simulations of buforin II and DesHDAP1 bound to repeating RNA sequence AU.

More replicates of these simulations could be run to average results. In addition, it would be consistent to collect experimental binding data for buforin II and DesHDAP1 bound to the repeating AU sequence.

As mentioned earlier, more experimental data should be collected for $1/C_{50}$ values to compare these values for each peptide and its all-arginine and all-lysine mutants. This may help us address the inconsistencies we have observed between experimental and computational data for relative DNA binding interactions of each peptide and its mutants.

With insights from this study and future studies on AMPs such as buforin II and DesHDAP1, it may be possible to engineer more potent analogs of currently known peptides. For example, a previous study has highlighted the important role of arginine in mediating protein-membrane interactions [7]. In this study, we also further confirmed arginine's importance in enhancing DNA binding for HDAPs. For peptides similar to buforin II and DesHDAP1, two peptides with mechanisms of action that involves both interactions with the target's lipid

membrane and then with the intracellular nucleic acids, these insights on arginine may be valuable for designing more effective mutants. Lastly, the systematic approach used in this study that involved combining computational and experimental methods appeared to be effective in providing insights as well as structural explanations for various observations. Thus, this may be a possible approach to characterize structures and/or interactions of similar biomolecular complexes.

References

[1] H.S. Tsao, S.A. Spinella, A.T. Lee, D.E. Elmore, Design of novel histone-derived antimicrobial peptides, Peptides 30 (2009) 2168-2173.
[2] M. Wenzel, A.I. Chiriac, A. Otto, D. Zweytick, C. May, C. Schumacher, R. Gust, H.B. Albada, M. Penkova, U. Kramer, R. Erdmann, N. Metzler-Nolte, S.K. Straus, E. Bremer, D. Becher, H. Brotz-Oesterhelt, H.G. Sahl, J.E. Bandow, Small cationic antimicrobial peptides delocalize peripheral membrane proteins, Proc Natl Acad Sci U S A 111 (2014) E1409-1418.
[3] Y. Fang, W. Zhong, Y. Wang, T. Xun, D. Lin, W. Liu, J. Wang, L. Lv, S. Liu, J. He, Tuning the antimicrobial pharmacophore to enable discovery of short lipopeptides with multiple modes of action, Eur J Med Chem 83 (2014) 36-44.
[4] S. Bandyopadhyay, M. Lee, J. Sivaraman, C. Chatterjee, Model membrane interaction and DNA-binding of antimicrobial peptide Lasioglossin II derived from bee venom, Biochem Biophys Res Commun 430 (2013) 1-6.
[5] F. Guilhelmelli, N. Vilela, P. Albuquerque, L.D. Derengowski, I. Silva-Pereira, C.M. Kyaw, Antibiotic development challenges: the various mechanisms of action of antimicrobial peptides and of bacterial resistance, Frontiers in Microbiology 4 (2013).
[6] S.C. Park, J.Y. Kim, C. Jeong, S. Yoo, K.S. Hahm, Y. Park, A plausible mode of action of pseudin-2, an antimicrobial peptide from Pseudis paradoxa, Biochim Biophys Acta 1808 (2011) 171-182.
[7] P. Nicolas, Multifunctional host defense peptides: intracellular-targeting antimicrobial peptides, FEBS J 276 (2009) 6483-6496.
[8] H. Kawasaki, S. Iwamuro, Potential roles of histones in host defense as antimicrobial agents, Infect Disord Drug Targets 8 (2008) 195-205.
[9] M.R. Yeaman, N.Y. Yount, Mechanisms of antimicrobial peptide action and resistance, Pharmacol Rev 55 (2003) 27-55.
[10] S. Macchi, G. Signore, C. Boccardi, C. Di Rienzo, F. Beltram, F. Cardarelli, Spontaneous membrane-translocating peptides: influence of peptide self-aggregation and cargo polarity, Sci Rep 5 (2015) 16914.

[11] R.M. Elder, A. Jayaraman, Molecular simulations of polycation-DNA binding exploring the effect of peptide chemistry and sequence in nuclear localization sequence based polycations, J Phys Chem B 117 (2013) 11988-11999.
[12] T. Niidome, N. Ohmori, A. Ichinose, A. Wada, H. Mihara, T. Hirayama, H. Aoyagi, Binding of cationic alpha-helical peptides to plasmid DNA and their gene transfer abilities into cells, J Biol Chem 272 (1997) 15307-15312.
[13] A. Patrzykat, L. Zhang, V. Mendoza, G.K. Iwama, R.E. Hancock, Synergy of histone-derived peptides of coho salmon with lysozyme and flounder pleurocidin, Antimicrob Agents Chemother 45 (2001) 1337-1342.
[14] C.B. Park, H.S. Kim, S.C. Kim, Mechanism of action of the antimicrobial peptide buforin II: buforin II kills microorganisms by penetrating the cell membrane and inhibiting cellular functions, Biochem Biophys Res Commun 244 (1998) 253-257.
[15] C.B. Park, K.S. Yi, K. Matsuzaki, M.S. Kim, S.C. Kim, Structure-activity analysis of buforin II, a histone H2A-derived antimicrobial peptide: The proline hinge is responsible for the cell-penetrating ability of buforin II, Proceedings of the National Academy of Sciences of the United States of America 97 (2000) 8245-8250.
[16] J.H. Cho, B.H. Sung, S.C. Kim, Buforins: histone H2A-derived antimicrobial peptides from toad stomach, Biochim Biophys Acta 1788 (2009) 1564-1569.
[17] E.T. Uyterhoeven, C.H. Butler, D. Ko, D.E. Elmore, Investigating the nucleic acid interactions and antimicrobial mechanism of buforin II, FEBS Lett 582 (2008) 1715-1718.
[18] Y. Xie, E. Fleming, J.L. Chen, D.E. Elmore, Effect of proline position on the antimicrobial mechanism of buforin II, Peptides 32 (2011) 677-682.
[19] S. Kobayashi, A. Chikushi, S. Tougu, Y. Imura, M. Nishida, Y. Yano, K. Matsuzaki, Membrane translocation mechanism of the antimicrobial peptide buforin 2, Biochemistry-Us 43 (2004) 15610-15616.
[20] Y. Lan, Y. Ye, J. Kozlowska, J.K. Lam, A.F. Drake, A.J. Mason, Structural contributions to the intracellular targeting strategies of antimicrobial peptides, Biochim Biophys Acta 1798 (2010) 1934-1943.
[21] K.E. Pavia, S.A. Spinella, D.E. Elmore, Novel histone-derived antimicrobial peptides use different antimicrobial mechanisms, Biochimica Et Biophysica Acta-Biomembranes 1818 (2012) 869-876.
[22] L. Pardo, N. Pastor, H. Weinstein, Selective binding of the TATA box-binding protein to the TATA box-containing promoter: analysis of structural and energetic factors, Biophys J 75 (1998) 2411-2421.
[23] W.D. Cornell, P. Cieplak, C.I. Bayly, I.R. Gould, K.M. Merz, D.M. Ferguson, D.C. Spellmeyer, T. Fox, J.W. Caldwell, P.A. Kollman, A second generation force field for the simulation of proteins, nucleic acids, and organic molecules (vol 117, pg 5179, 1995), Journal of the American Chemical Society 118 (1996) 2309-2309.
[24] J. Srinivasan, T.E. Cheatham, P. Cieplak, P.A. Kollman, D.A. Case, Continuum solvent studies of the stability of DNA, RNA, and phosphoramidate - DNA helices, Journal of the American Chemical Society 120 (1998) 9401-9409.
[25] F. Diez-Garcia, A. Chakrabartty, C. Gonzalez, D.V. Laurents, An Arg-rich putative prebiotic protein is as stable as its Lys-rich variant, Arch Biochem Biophys 528 (2012) 118-126.
[26] J.M. Sanders, M.E. Wampole, C.P. Chen, D. Sethi, A. Singh, F.Y. Dupradeau, F. Wang, B.D. Gray, M.L. Thakur, E. Wickstrom, Effects of hypoxanthine substitution in peptide nucleic

acids targeting KRAS2 oncogenic mRNA molecules: theory and experiment, J Phys Chem B 117 (2013) 11584-11595.
[27] J. Panecka, C. Mura, J. Trylska, Molecular Dynamics of Potential rRNA Binders: Single-Stranded Nucleic Acids and Some Analogues, Journal of Physical Chemistry B 115 (2011) 532-546.
[28] M.L. Radhakrishnan, Designing electrostatic interactions in biological systems via charge optimization or combinatorial approaches: insights and challenges with a continuum electrostatic framework, Theoretical Chemistry Accounts 131 (2012).
[29] H.W. Qi, P. Nakka, C. Chen, M.L. Radhakrishnan, The effect of macromolecular crowding on the electrostatic component of barnase-barstar binding: a computational, implicit solvent-based study, PLoS One 9 (2014) e98618.
[30] K. Luger, A.W. Mader, R.K. Richmond, D.F. Sargent, T.J. Richmond, Crystal structure of the nucleosome core particle at 2.8 A resolution, Nature 389 (1997) 251-260.
[31] J. Dolenc, S. Gerster, W.F. van Gunsteren, Molecular dynamics simulations shed light on the enthalpic and entropic driving forces that govern the sequence specific recognition between netropsin and DNA, J Phys Chem B 114 (2010) 11164-11172.
[32] H.Y. Liu, X. Zou, Electrostatics of ligand binding: parametrization of the generalized Born model and comparison with the Poisson-Boltzmann approach, J Phys Chem B 110 (2006) 9304-9313.
[33] B.N. Grant, E.M. Dourlain, J.N. Araneda, M.L. Throneberry, L.A. McFail-Isom, DNA phosphate crowding correlates with protein cationic side chain density and helical curvature in protein/DNA crystal structures, Nucleic Acids Res 41 (2013) 7547-7555.
[34] J.M. Crowet, L. Lins, S. Deshayes, G. Divita, M. Morris, R. Brasseur, A. Thomas, Modeling of non-covalent complexes of the cell-penetrating peptide CADY and its siRNA cargo, Biochim Biophys Acta 1828 (2013) 499-509.
[35] K.J. Cutrona, B.A. Kaufman, D.M. Figueroa, D.E. Elmore, Role of arginine and lysine in the antimicrobial mechanism of histone-derived antimicrobial peptides, FEBS Lett 589 (2015) 3915-3920.
[36] S. Balakrishnan, M.J. Scheuermann, N.J. Zondlo, Arginine mimetics using alpha-guanidino acids: introduction of functional groups and stereochemistry adjacent to recognition guanidiniums in peptides, Chembiochem 13 (2012) 259-270.